Extended Modeling Studies of the TWA 800 Center-Wing Fuel Tank Explosion

Melvin R. Baer and Robert J. Gross

Approved for public release; further dissemination unlimited.

Sandia National Laboratories

Extended Modeling Studies of the TWA 800 Center-Wing Fuel Tank Explosion

Melvin R. Baer and Robert J. Gross
Engineering Sciences Center
Sandia National Laboratories
P. O. Box 5800
Albuquerque, New Mexico USA 87185-0836

Abstract

This report summarizes modeling studies supported by a second phase of quarter-scale testing for the NTSB investigation of the TWA Flight 800 accident. In this study, fuel-air tests were conducted to replicate earlier tests to assure repeatability of results. The quarter-scale test tank was redesigned to use heated Jet-A fuel/air mixtures at reduced ambient pressures. Although combustion explosions are observed using Jet-A air mixtures, the combustion behavior is distinctly different than the simulant fuel. As opposed to the quarter-scale simulant fuel test where quench was absent, quenching behavior is seen in almost all tests with Jet-A fuel. To assess the effect of incomplete combustion and its implications to the full-scale center wing fuel tank in TWA 800, a series of two compartment tests were conducted. A combined experimental/computational approach is used to define a quench criterion which can then be applied in a full-scale CWT simulation.

Acknowledgements

Table of Contents

List of Figures

Introduction

The National Transportation Safety Board (NTSB) sponsored a series of quarter-scale tests as a part of the investigation of the TWA Flight 800 accident. The purpose of these tests was to provide data for computer model development. The models could then be used to assist in determining the most probable ignition location that is consistent with the damage in the recovered center wing tank (CWT). The initial studies demonstrated that weak ignition of a lean fuel-air mixture in the CWT produces a combustion event sufficient to cause structural damage in the tank[1]. The nature of the explosive event involves the development and propagation of accelerated turbulent flames due to the interaction of fluid mechanics and combustion in the multiple compartments of the CWT.

The complex nature of reacting turbulent flow described by a detailed first-principle simulation of the explosion is beyond any known computational capability. Furthermore, much of the underlying combustion physics is not well understood. Two modeling activities were sponsored by the NTSB. The effort undertaken by Christian Michelsen Research laboratory (CMR) uses an existing computational fluid dynamic code, FLACS[2], to predict the flame propagation and the internal tank pressures following ignition. The approach used by Sandia National Laboratories (SNL) is based on a description that does not require resolving flow details but rather determines pressure histories from global mass, momentum, and energy balances[3]. Flame propagation is represented as a moving interface that separates burned and unburned gases and the rate of flame spread is governed by a flame law dictated by experimental data and engineering correlations[4].

Although these two modeling approaches can replicate some aspects of the experimental observations, both models incorporate approximations or submodels that require "parameter adjustments" to achieve agreement with test data. Predictability of a model often requires extensive testing and evaluation to assure that the descriptions include all relevant aspects of the physics. To validate a model, the experimental data must be representative of actual conditions. As in engineering analysis and modeling, approximations are often introduced in experimental investigations because the replication of actual conditions is usually impossible, time-consuming or prohibitively expensive.

In the initial TWA Flight 800 investigation quarter-scale testing program, a simulant fuel was used to reduce complexity and provide well-defined initial conditions for the modeling studies[5]. Laboratory tests at Cal Tech suggested that the combustion behavior of heated gaseous Jet-A fuel-air mixtures can be replicated using a mixture of hydrogen-propane premixed with air. The choice of this simulant fuel-air mixture is based on reproducing burn rates and overpressures in laboratory-scaled vessels[6]. The use of the simulant fuel bypasses the difficulties associated with heating liquid jet fuel, hence, the quarter-scale test apparatus required minimal external environmental control.

During the first phase of this testing, thirty quarter-scale tests were conducted whereby various effects such as ignition location, fuel tank compartment configuration and strong versus weak panel walls[7] were studied. On the basis of these quarter-scale tests, the CMR and SNL computational models were "adjusted" to conditions relevant to the turbulent combustion of simulant fuel.

Some important observations were noted during the first phase of tests. Several earlier tests included a liquid Jet fuel layer at the bottom of the tank and photographic observations showed that the induced motion associated with the gas-phase combustion was sufficient to strip the liquid fuel off of the tank floor and disperse it as an aerosol. Since droplet combustion is distinctly different from gas-

phase reaction, the role of the liquid fuel remain unclear. The simulant fuel was selected entirely based on fluid dynamic and thermodynamic arguments associated with the vapor phase rather than those of the liquid fuel. Additionally, replication tests were not performed in the early phase of testing to assure repeatability of results to indicate what is predictable by modeling. Thus, several questions arose. Is the relevant combustion physics of the explosive event in the actual CWT geometry appropriately represented in the quarter-scale testing? Is the explosive event deterministic? These important questions had to be answered before the modeling can be assured as an appropriate "diagnostic" tool in the accident investigation.

In light of these concerns, the second phase of testing focussed on repeatability tests using the simulant fuel followed by tests with heated Jet-A fuel.The quarter-scale tank configuration was modified to allow vaporization and mixing of heated jet fuel with air. The fuel-air mixture was recirculated throughout the test chamber to bypass any stratification effects[†]. The test chamber was electrically heated and sealed to allow reduced pressure consistent with the 0.6 atm. condition of the TWA-800 accident. The test apparatus was contained in an insulated enclosure to control ambient condition temperatures within $2\ ^0C$.

Twelve tests using the simulant fuel were performed to reproduce earlier test results. In all of these tests the quarter-scale configuration incorporated structurally-strong partitions between compartments. Hence, the complexity of resolving coupled structural response and the combustion was purposely avoided. Most of these tests produced overall pressure histories similar to those observed in earlier tests. However, there were differences associated with the time to the onset of accelerated combustion and the pressure differentials across adjacent compartments. Since the earlier tests were conducted during the late fall and winter months at Denver, Colorado, it is likely that the differences in overpressures were due to variations in ambient conditions.

The next nineteen tests investigated flame propagation in a heated jet fuel-air mixture These tests investigated flame propagation at varied fuel temperatures of 40 °C, 45 °C and 50 °C. Figure 1 displays an overlay of experimental overpressures for two tests using heated Jet-A fuel at 40 °C and 50 °C. In all of the earlier tests with simulant fuel, flame propagation occurred throughout the tank and accelerated burning produced rapid pressure rise in all of the compartments. However, for heated Jet-A fuel, flame propagation is different because inter-compartment propagation of the flames usually involved some degree of quenching, re-ignition and/or incomplete combustion. Contrary to the earlier observations, there appears to be a strong dependence on ignition location (as illustrated in Figure 1) and greatly different pressure histories are observed when the flames propagate (or fail to propagate) from compartment to compartment. This behavior suggest that *higher* pressure differentials can potentially be realized if combustion takes place in a compartment and fails to propagate into an adjacent region. Clearly, the nature of this quench behavior and the appropriate scaling of this effect had to be addressed before any pressure loading history can be confidently predicted for the structural response of the CWT. From a modeling viewpoint, unraveling the myriad of combustion behavior from only global experimental pressure-time data poses an extremely difficult task.

---

†In the replication flights[8], thermocouple measurements in CWT confirmed that thermal gradients existed in the CWT. It is highly probable that TWA 800 CWT tank experienced similar nonuniform temperature and concentration fields. These exact conditions must be recognized as impractical to reproduce at a reduced scale geometry.
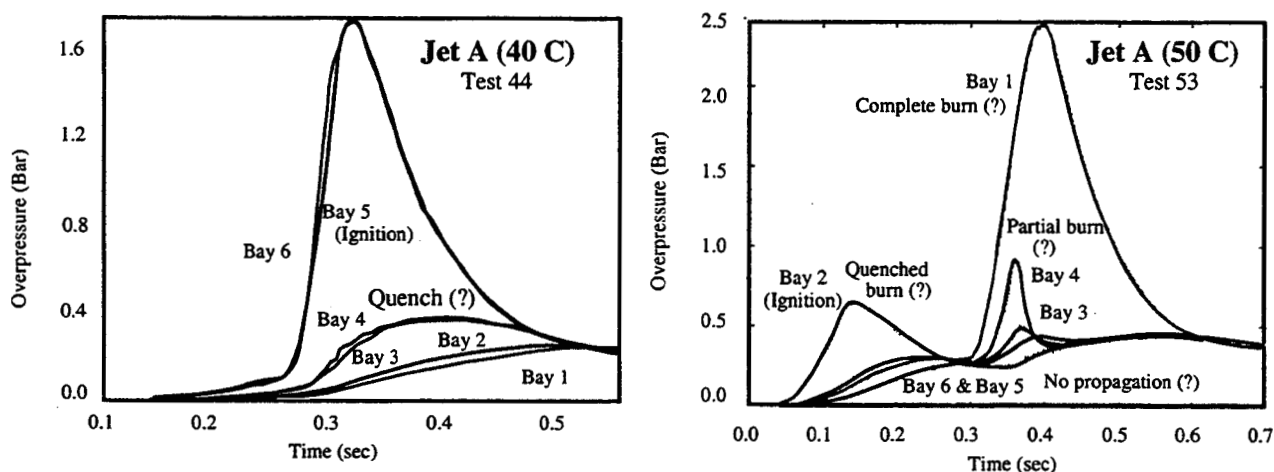
Figure 1. Experimental measurements of overpressures in quarter-scale tests using heated Jet-A at 40 °C (ignition in bay 5) and 50 °C (ignition in bay 2)

In this series of testing, the study centered on quench behavior of flame propagation in the multiple compartments of the CWT. Although gas-sampling techniques were incorporated in these tests[9], an accurate determination of the composition of the vapor fuel-air mixture in the tank space remained an unresolved problem. Initial conditions are a very important input to any modeling, especially when it was demonstrated that varied sources of Jet -A fuel produced dramatically different combustion behavior. Thus, single bay tests were conducted to provide information on flame speed and overall pressure rise at varied ambient temperatures for the ARCO jet fuel. Repeatability tests confirmed that similar transient overpressures occur in the quarter-scale configuration.

As suggested by the pressure histories given in Figure 1, flame propagation into a multicompartment tank involves a very complex flow that triggers and sustains reaction in certain compartments and quenches or partially-burns in others. To unravel the nature of incomplete combustion behavior from the experimental pressure histories in the quarter-scale tank, modeling provides a means to determine the details of the flow field near openings connecting compartments. High speed photography was attempted in several tests, however, these observations produced very limited visual information on combustion behavior because the induced turbulence and liquid fuel dispersion obscured the direct observations. It became apparent that the geometry had to be simplified to a two compartment configuration because it was exceedingly difficult to determine when the flames quenched and/or re-ignited in a multiple compartment configuration. (As an example of the variety of possible combustion states in a six compartment configuration there are 64 combinations of burn/ quench possibilities!)

In the two compartment tests the ignition location was fixed at the center of an ignition compartment and a flame propagates toward a single opening to a receiver compartment. As suggested by prior studies, many effects such as ignition location or induced turbulence levels influence propagation behavior. A limited set of tests was conducted with the intent of determining the nature

of quench and its scaling law. Six tests (including replications) were done in the two compartment configuration varying the appropriate length scale of the connecting flow passage.

In the following section, a model of flame quench due to the effects of flow strain through an opening is presented. The characteristics of the flow field associated with flame propagation are determined by combining experimental overpressure measurements and modeling to quantify an appropriate quenching criterion. The data for two-compartment quarter-scale tests provides a means to assess quench behavior in the full-scale tank geometry. Revised flame propagation data for Jet-A fuel-air combustion is then used to simulate a fuel-air explosion in the full scale fuel tank. In light of indeterminate initial conditions and the weak basis of few experimental tests on quench behavior, the model results must be regarded with some uncertainty. Much remains to be clarified on the turbulent flame propagation and incomplete combustion behavior of Jet fuel-air mixtures.

A Model for Flame Quenching

When a laminar flame moves into an unburned region of premixed combustible gases, it continues to propagate because a small amount of heat is transferred ahead of the flame causing ignition and self-sustained reaction of the unreacted gases. The structure of the flame dictates how much energy is passed forward of the flame. If temperature gradients are greatly modified, the flame can cease to propagate and it then extinguishes.

Extensive study of flame quenching has been done with the goal of preventing and mitigating industrial explosions. A "maximum-experimental-safe-gap" (MESG) has been suggested that identifies the critical minimum dimensions of gaps or holes in enclosure walls through which an explosion can be transmitted. Although an extensive database of experimental measurements has been obtained[10], a fundamental understanding of quenching behavior still does not exist and the MESG concept is not a well established or accepted criteria.

Several mechanisms can cause quenching of flame propagation. If excessive heat transfer takes place in the preheat zone of a flame, thermal dissipation prevents self-sustained reaction. Previous research has established a "quenching diameter" based on the propagation of flames in thin capillary tubes whereby conduction heat transfer to the walls alters the diffusive-convective region of the flame sufficient to cause quenching. It has been observed that the quenching diameter for hydrocarbon-air mixtures is nominally of the order of a few millimeters[11]. In the quarter-scale tests using Jet-A fuel-air mixtures, much larger holes caused quenching, hence, the mechanism of quenching appears to be fundamentally different than that entirely based on heat transfer arguments.

There are other mechanisms which alter the structure of the flame during propagation. As a flame propagates it induces a flow because product gases expands due to the energy added by reaction. The rate of energy release has a strong effect on flame propagation and a measure of the temperature sensitivity of the overall reaction and the extent of reaction completeness is represented by the Zeldovich number. Fluid mechanics also has a major influence on flame structure, especially when the characteristic time scales of the flow are of the same order as the chemical kinetics[12]. The Damköhler number represents the ratio of a time scale associated with chemical reaction to the local flow scale. Strong interactions between flow and reaction can be expected when the Damköhler number approaches unity.

In contrast to the laminar propagation in capillary tubes, turbulent flame propagation is observed in the quarter-scale tests (and expected in the full-scale CWT) and the appropriate length scales are those associated with the turbulence[13]. As the flame propagates from compartment to compartment, through small holes, turbulent jets produce distorted flames. It is this flow strain which is suspected to be the likely cause of the flame quenching.

A small-scale laboratory apparatus has been developed at the University of Bergen[14] whereby a flame propagates from a primary chamber to a receiver volume through a circular hole of varied diameter. At some critical diameter a flame fails to propagate into the receiver volume at a fixed distance from a spark ignition source to the receiver volume entrance. Go/no-go results shows a strong dependence of the critical hole diameter for explosive transmission with the ignition distance. These experiments clearly indicate that flame transmission depends on the local flow conditions at the hole location and flow effects extinguishes the flame as it is pushed through the connecting flow passage. Unfortunately, these lab-scaled tests have only examined propane-air mixtures, not the Jet-A fuel-air mixtures of interest in this study. As one might expect, fuel type and stoichiometry are also important factors in determining quench behavior. Additionally, the effect of dispersing a liquid fuel on quench behavior is unknown.

At some appropriate scale, turbulent premixed flames consist of laminar flames that are subjected to flow strain as a consequence of local velocity fluctuations. The general definition of flame stretch for planar flames is the time derivative of the logarithm of the area of the flame surface. Bradley[13] uses this definition to define a non-dimensional number called the Karlovitz number, $\mathcal{K}$. This strain rate is normalized by the chemical reaction time associated with the flame sheet (this number is the inverse of the Damköhler number):

$$\mathcal{K} \equiv \frac{1}{S_f} \frac{dS_f}{dt} \frac{\delta_l}{u_l} \tag{1}$$

where S_f is the laminar flame surface area, δ_l is the laminar flame thickness and u_l is the laminar burn velocity. For turbulent flames, the strain rate of the flame is related to the turbulent intensity, u', (a velocity state associated with the mean fluctuating flow field) and the Taylor microscale, λ (a length scale associated with turbulent flow strain rate) as follows:

$$\frac{1}{S_f} \frac{dS_f}{dt} \sim \frac{u'}{\lambda}. \tag{2}$$

For an isotropic turbulent flow, the Taylor microscale is related to the integral scale, L, (a length scale associate with the physical extent of the turbulence) as follows:

$$\frac{\lambda^2}{L} \sim \frac{40.4\nu}{u'} \tag{3}$$

where the kinematic viscosity of the gas mixture is denoted as ν. The laminar flame thickness is estimated as:

$$\delta_l \sim \frac{\nu}{u_l}. \tag{4}$$

To define the turbulence characteristics of the receiver volume, researchers at CMR have suggested that the turbulent intensity is proportionate to the local flow velocity, u_{jet}, at the entrance to the receiver volume and the integral scale is scaled to the hole diameter, d_{jet}[15]. Using these arguments the Karlovitz number for *isotropic* turbulent propagation is then defined as:

$$\mathcal{K} \propto (\nu u_{jet}^3 / d_{jet})^{1/2} u_l^{-2}. \tag{5}$$

Since the Karlovitz number is related to the Damköhler number, it is further postulated that quenching occurs at a critical value of $\mathcal{K}$. If this criterion is valid, a scaling law for quenching is determined and quenching in the full scale CWT may be assessed.

As a flame propagates toward an opening to an adjacent region, a jet is formed at the receiver entrance and the induced flow stretches the flame prior to its arrival. Thus, flow strain effects can originate ahead of the opening and additional flame strain takes places as it passes through the opening. The near field flow associated with a jet is distinctly different than isotropic turbulence. The Karlovitz criteria, given as equation 1, can be modified to treat flow strain representative of turbulent jet flow.

Turbulent jets have been extensively studied during the past fifty years and a wealth of experimental data exists on the structure of these flows[16]. Near the entrance of a jet the velocity at the center remains nearly constant to a distance, z_c. The near field of the jet is referred as the potential core region. Thereafter, the flow expands and eddies form to mix with ambient gases. When a planar flame impinges on the entrance to the circular opening, the flame surface expands to the extent of the potential core. Thereafter, the flame is engulfed by the surrounding turbulent field.

For a round jet, the potential core is represented as a conical surface area, A_{core} having a base radius equal that of the orifice opening and a base height equal to the potential core length. As one expects, a high speed flow velocity, u_{jet}, exists at the entrance and the time scale over which the flame changes its initial surface area, A_{jet} to A_{core} is z_c / u_{jet}. Thus, the flame strain rate is determined as:

$$\frac{1}{S_f} \frac{dS_f}{dt} \sim \frac{(A_{core} - A_{jet}) u_{jet}}{A_{jet} z_c}. \tag{6}$$

Similar to the isotropic turbulence criteria, the chemical time is assumed to scale to the flame thickness divided by the burn velocity. (It is noted that for a multicomponent fuel-air mixture, this may not be an appropriate measure of the chemical time scale and the Zeldovich number should be included in this determination.) Experimental measurements in round jets suggest that the length of the potential core region directly scale with orifice diameter: $z_c / d_{jet} \sim 6 \rightarrow 8$ and applying simple geometric relationships for the surface areas results in a different Karlovitz number:

$$\mathcal{K}_{jet} \propto (2\nu u_{jet} / d_{jet}) u_l^{-2}. \tag{7}$$

Bradley suggests that a critical quench criteria includes the effects of molecular transport using the Lewis number, Le and a critical value of $\mathcal{K}_{jet}Le$ defines the boundary between propagating turbulent premixed flames and quenched behavior. It is noted that for the case of a planar jet, depicted in Figure 2, the same criterion is determined whereby the slot width replaces the orifice diameter.
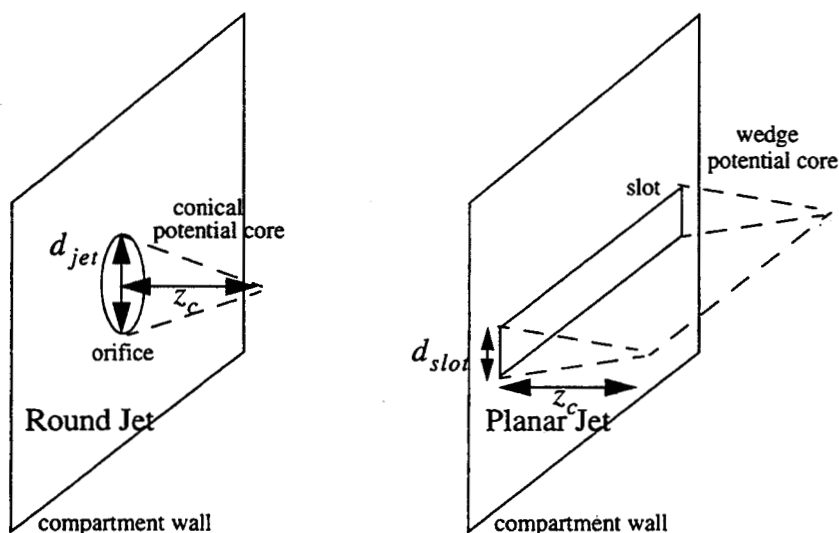

Figure 2. Representative geometries for the jet flows in round and slot orifices.

With this foundation for scaling the quench effects due to flow strain, it remains to determine a critical dimensional number appropriate to Jet-A fuel-air mixtures. The quarter-scale tests using the two compartment configuration provide a means for this determination. In these tests only the overpressure is measured and the details of the flow near connecting flow passages is determined by modeling. All of the details of the modeling have been discussed in a prior report[3] and will not be repeated here.

In the section to follow, the quarter-scale test data is used to determine a quenching criteria which is then applied to a model of the full scale CWT. Since this criteria is determined by modeling, the validity of this assessment ultimately hinges on the accuracy of the initial conditions. Furthermore, since only a limited set tests at a single ignition location were done to bound quenching behavior, any uncertainty of the modeling must also consider the limitations of the experimental test data.

Single Compartment Modeling

In contrast to the well-defined composition of the simulant fuel, Jet-A liquid fuel is a complex blend of hydrocarbons. The gaseous constituents that vaporized from a liquid layer and mix with low pressure air greatly depend on the thermal field, mass-loading and volatility of the liquid. The combustion characteristics of these gaseous constituents are critical aspects of modeling because the rate of flame propagation and the maximum overpressure are influenced by initial conditions. Laboratory-scale tests were conducted to define combustion parameters, however, the composition of Jet-A fuel used in these earlier tests was likely to be different than that used in the quarter-scale tests. Gas sampling was attempted with only marginal success and much uncertainly remained in properly defining initial conditions. Also, heat transfer effects depend on the geometry of the test chamber. Hence, a series of single compartment tests were conducted using ARCO Jet-A to provide key

combustion and heat transfer parameters for the quarter-scale test chamber without resolving flow effects associated with interacting compartments. Replication tests were done to assure that the flame propagation behavior is deterministic.

Two single compartment tests, 61 and 62, served to characterize the combustion behavior of ARCO Jet-A/air at 50 °C and 0.585 atm. Based on prior fuel characterization studies[6], Jet-A fuel is modeled as C_9H_{20} with a heat of formation of -54.3 [Kcal/mole] and the fuel/air mass ratio is estimated to be 0.06. Ignition of the mixture is initiated at the center of the test chamber whereupon a spherical combustion wave grows to consume premixed fuel and air. Expansion of the reaction products induces overpressure in the test chamber. Following the completion of combustion, the chamber pressure falls due to cooling as the hot gases interact with the confinement walls. The experimental and the predicted overpressure are overlaid in Figure 3. All aspects of the combustion event including the initial
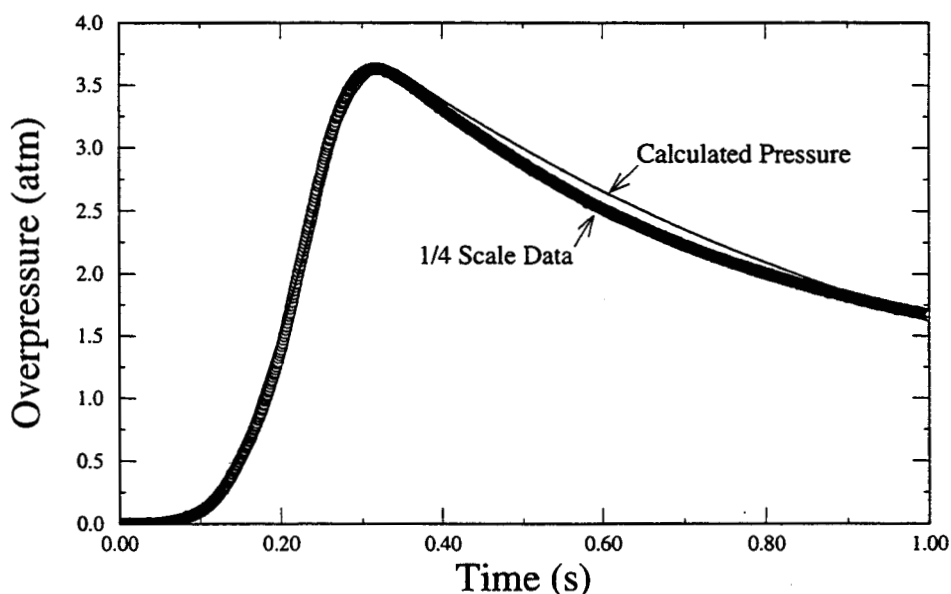

Figure 3. Overpressure versus time for Quarter-Scale Experiment 61

pressure buildup, time to maximum overpressure, and the late-time pressure drop due to heat loss are well predicted in the simulation. Nearly identical pressure histories were measured to assure repeatability of the combustion event. Each single compartment test incorporated several gauges that measured pressure histories which overlaid one another, again verifying the validity the low Mach number combustion approximation of the modeling. The early time t^3 characteristic of the pressure corresponds to the spherical growth of a laminar flame. The laminar burn velocity at this early time was determined to be 37 cm/s which is consistent with laboratory-scale tests.[†]

Tests 71, 72, and 73 are single compartment experiments conducted at identical conditions of 40°C and 0.585 atm. An overlay of the measured pressure histories suggested repeatability of results. At various initial temperatures, different fuel species reach equilibrium with the ambient air. Hence,

---

[†]The prior modeling of the simulant fuel tests prescribed the flame velocity instead of the burn velocity in this work. Reference 3 provides the derivation of the description relating these quantities.

the laminar burn velocity changes due to variation in composition and mean temperature. At this lower temperature condition, the burn velocity is estimated to decreases to approximately 15 cm/sec.
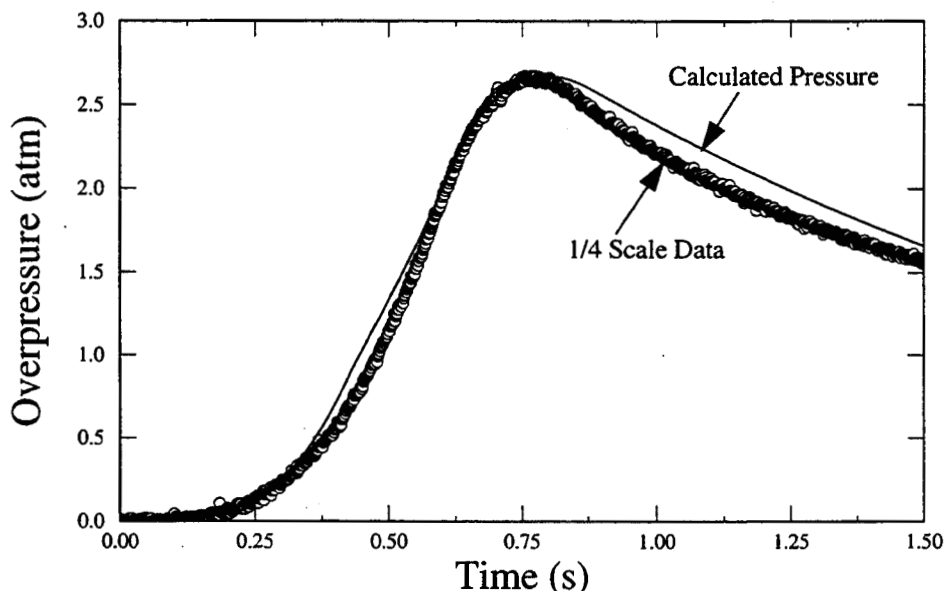

Figure 4. Overpressure versus time for Quarter-Scale Experiment 73

Since the lower burn velocity induces less motion of the expansion products and one expects reduces convective heat losses. The convective heat loss incorporated in the model assuming a constant heat transfer coefficient during the entire combustion event. At 40 °C the heat transfer convective coefficient for the quarter scale test chamber is estimated to be 112,000 [erg/(cm^2 sec.)] whereas, at 50 °C, the coefficient is estimated to be 186,000 [erg/(cm^2 sec.)]. The Edward's exponential wide-band model is retained in estimating thermal radiation losses. An overlay of the experimental and the predicted pressure histories for Test 73 is given in Figure 4. At 40 °C the maximum overpressure is approximately 2.6 atm. as opposed to 3.6 atm. at 50 °C. The modeling suggests that much of the difference in maximum overpressure is due to the effects of heat transfer (multiple runs varying *only* the heat transfer coefficient confirm this argument). With an acceptable calibration of the combustion modeling in the single compartment chamber, the modeling is then applied to flame propagation in the quarter-scale multiple compartment configuration.

Two Compartment Modeling

As discussed in the introduction, the combustion of Jet-A/air mixture is observed to be markedly different than that of the simulant fuel due to the complex interactions of fluid mechanics and chemical reaction. Tests in the multiple compartment configurations consistently indicated that the flame propagation is incomplete and often quenched as it spread from compartment to compartment. Unfortunately, the path of propagation throughout the multiple compartment quarter scale test could not be unraveled solely from the pressure measurements. To simplify the analysis and data interpretation, the quarter-scale chamber was configured to two compartments in which the fuel-air mixture is ignited in one compartment and the flame is propagated toward a single orifice connecting a receiving compartment. The diameter and shape of the orifice is varied in an attempt to define conditions which cause quenching of the flame. Nine two-compartment tests were conducted, seven at 50 °C and two at 40 °C. Three of the 50 °C tests are replicate tests. Experimental repeatability throughout this test series is excellent. Four 50 °C tests incorporated circular holes of diameter 5.08 cm, 3.81 cm, 2.54 cm and a 0.635 cm by 5.08 cm slot. The two 40 °C tests considered flame propagation toward a 0.635 cm by 5.08 cm slot and a 2.54 cm diameter hole.

Test 63 (and the replication test 65) is a two-compartment 50°C test having a single 5.08 cm diameter hole connecting the ignition compartment (compartment 2) and the receiver compartment (compartment 1). Flame propagation passed through this orifice and both chambers pressurized to approximately the same pressure maximum. The experimental and the predicted overpressures are given in Figure 5. A history tracer is included in the computation at the orifice location and all of the characteristics of the flow are monitored to define the local jet Karlovitz number as given in Figure 6. As the flame propagates in the ignition compartment, a jet flow is induced at the orifice location due to gas motion occurring ahead of the flame front. The flame reached the orifice at 0.086 sec. whereupon the jet Karlovitz number is calculated to be approximately 1.6.
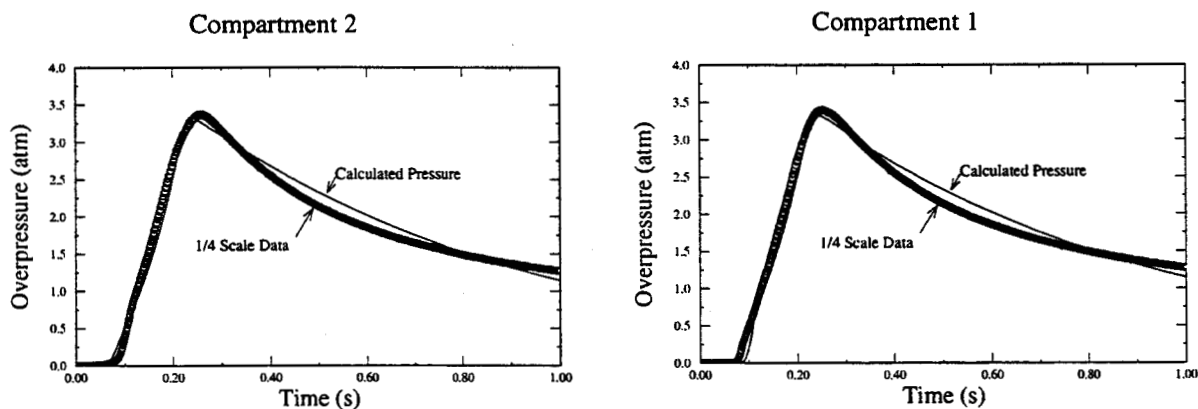

Figure 5. Overpressure versus time for Quarter-Scale Experiment 63

Test 64 (and the replication test 66) is a two compartment test incorporating the 0.635 cm by 5.08 cm slot. Quenching occurred during this test as evident by the pressure histories shown in Figure 7. The experimental pressure in the receiver compartment (Compartment 1) reaches a peak
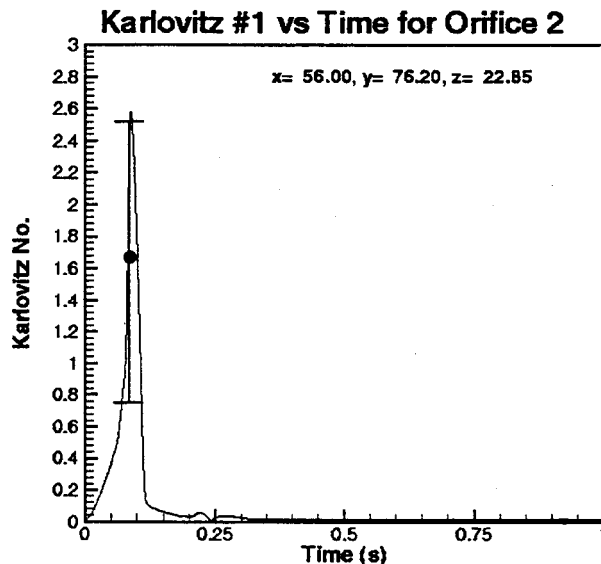
Karlovitz #1 vs Time for Orifice 2

x= 56.00, y= 76.20, z= 22.85

Figure 6. Jet Karlovitz number versus time for Quarter-Scale Experiment 63

pressure only about 1/7th that of the ignition compartment and the pressure difference between compartments is approximately 3 atm. Figure 7 overlays the predicted computational pressures assuming that no combustion occurred in Compartment 1. A higher overpressure is predicted in the ignition compartment and a lower pressure is calculated in the receiver compartment than experimentally observed. Revised calculations were made with variations in orifice area and discharge coefficient. Unacceptably large modifications of these conditions strongly suggested that an instantaneous quench assumption is incorrect. Alternatively, it is postulated that a partial burn occurs in the receiver compartment. Figure 8 displays an overlay of model prediction with experimental data for a case where the flame continues to propagate from the ignition bay to the receiver bay but quenches after 0.15 sec. (the flame first impinges the receiver bay at 0.107 sec.). The resulting calculation is consistent with the experimental observations without modifying any orifice flow characteristics. This strongly suggested that quench behavior for this case is not instantaneous when the flame impinges the orifice. Photographic observation of the propagation was attempted but was not successful in capturing the quench event. Prior to reaching the orifice the flame surface is highly stretched and rapid shear possibly breaks the flame sheet into individual flamelets that decelerate to extinction. In this configuration the quench process occurs over 43 milliseconds. Tracer information is included in the calculation and the jet Karlovitz number is given in Figure 9. At the time of flame impingement the Karlovitz number is approximately 13.
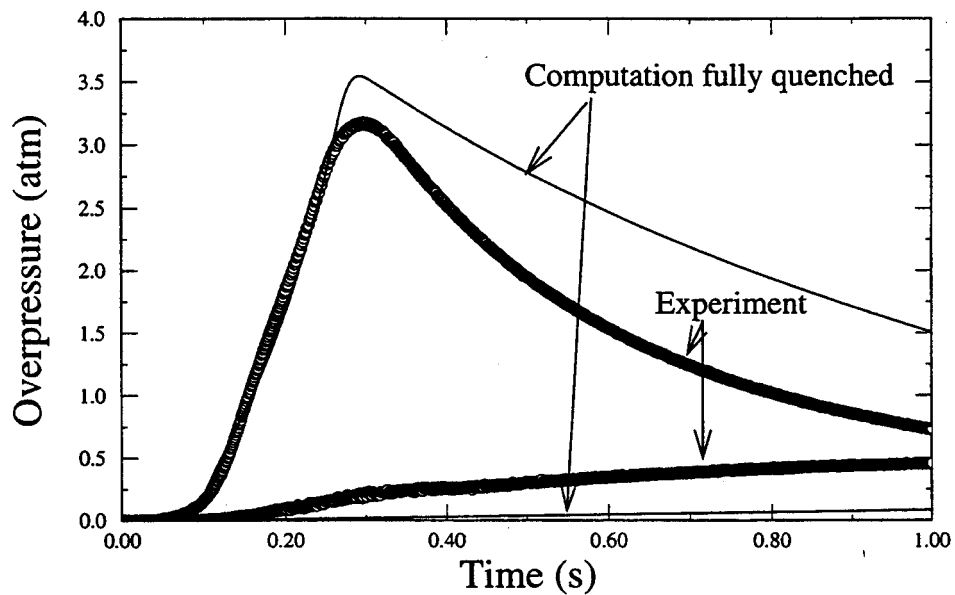
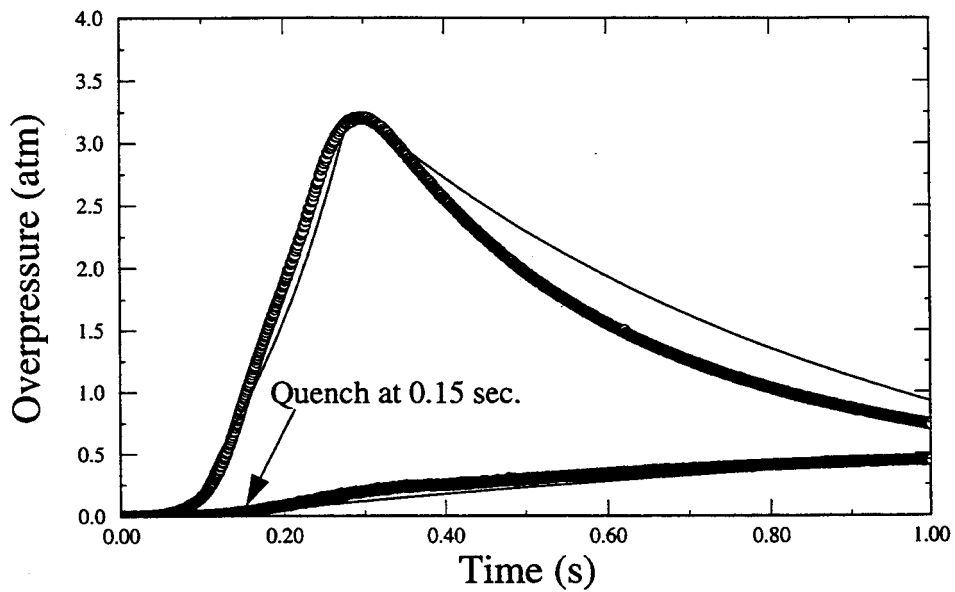Figure 7. Overpressure versus time for Quarter-Scale Experiment 64

Figure 8. Overpressure versus time for Quarter-Scale Experiment 64

Karlovitz #1 vs Time for Orifice 2
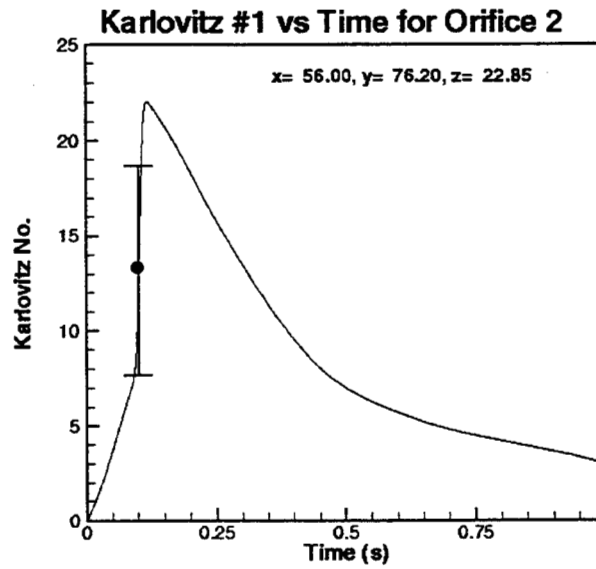
x= 56.00, y= 76.20, z= 22.85

Figure 9. Jet Karlovitz number versus time for Quarter-Scale Experiment 64
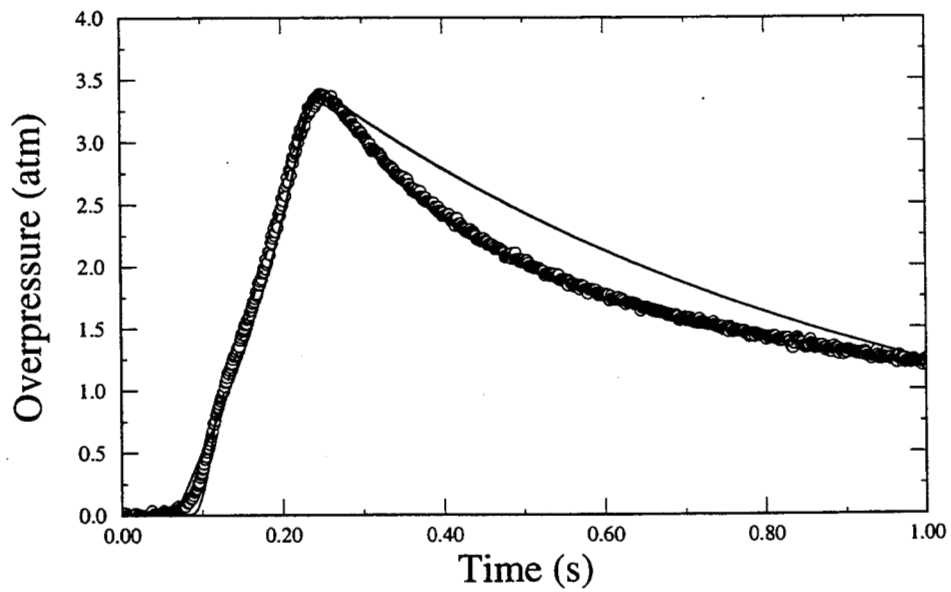
Figure 10. Overpressure versus time for Quarter-Scale Experiment 79

Additional tests were conducted in an attempt to define a "critical" hole diameter that would cause quenching. Test 79 is a two compartment test having a 3.81 cm diameter hole between the compartments. Figure 10 displays an overlay of the experimental and computational results for the 3.81 cm orifice test. Quenching did not occur in this test and similar overpressures are generated in each compartment. Figure 11 shows the resulting jet Karlovitz number for this test (flame impingement occurred at 0.08 sec.). These calculations suggest that the critical jet Karlovitz number for quenching must be greater than 1.0.

Karlovitz #1 vs Time for Orifice 2
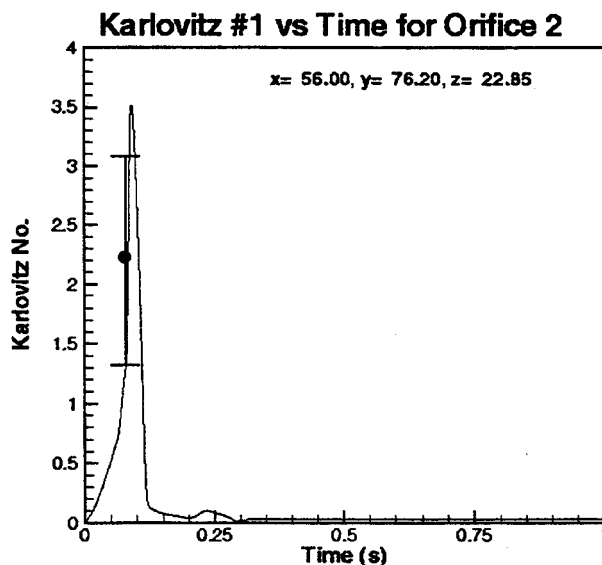
x= 56.00, y= 76.20, z= 22.85

Figure 11. Jet Karlovitz number versus time for Quarter-Scale Experiment 79

At this point in the two-compartment testing quenched flame behavior is observed to take place in configurations having a single orifice between 3.81 cm and 0.635 cm. Test 78 incorporated an intermediate size orifice diameter of 2.54 cm. The calculated and experimental overpressures are shown in Figure 12. The simulation did not consider any quench behavior despite the obvious indication seen experimentally. The jet Karlovitz number versus time for this test is display in Figure 13. At the time of flame impingement, t= 0.08 sec., the Karlovitz number is estimated to be 2.0. Thus, a critical jet Karlovitz number is bounded between 2.0 and 13.0.
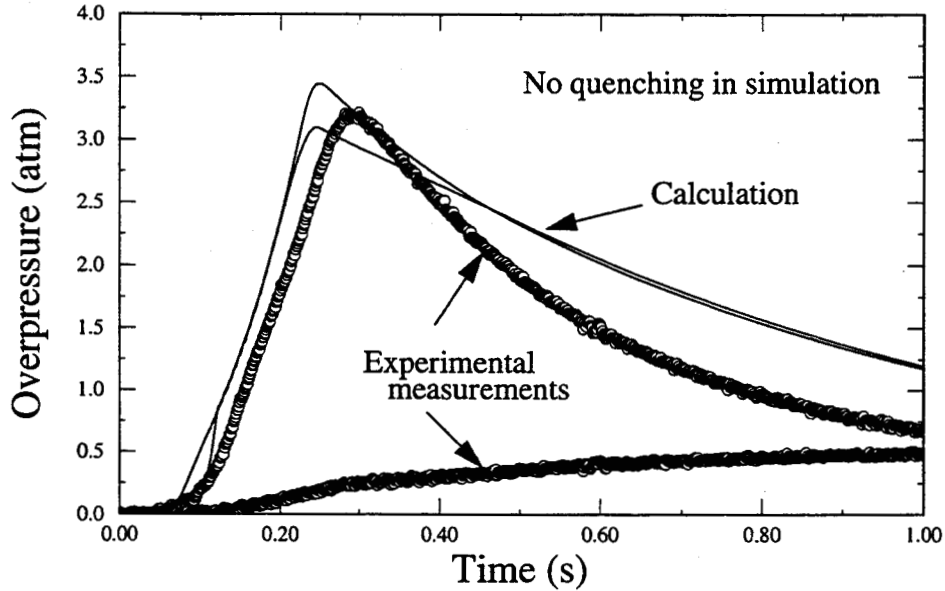
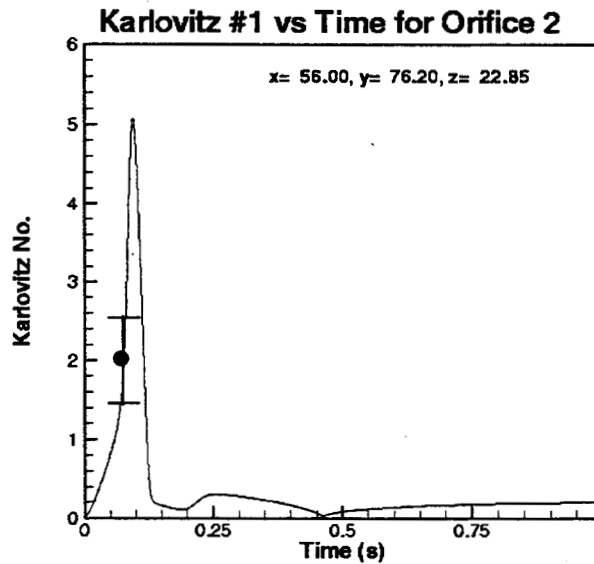Figure 12. Overpressure versus time for Quarter-Scale Experiment 78

Figure 13. Jet Karlovitz number versus time for Quarter-Scale Experiment 78

Two 40 °C two-compartment tests were conducted to examine the effect of initial fuel temperature on quench behavior. Test 77 used a 5.08 cm diameter orifice and a comparison of experimental and calculated overpressure are shown in Figure 14. At this condition flame propagation occurs in both compartments and the jet Karlovitz number versus time is displayed in Figure 15. At the time of flame impingement (0.25 sec.), the Karlovitz number is about 4.0.

Figure 14. Overpressure versus time for Quarter-Scale Experiment 77

Figure 15. Jet Karlovitz number versus time for Quarter-Scale Experiment 77

The second 40 °C test incorporated a 0.635 cm by 5.08 cm slot. Quenched propagation in the receiver compartment is observed at this condition. Experimental and computed overpressures for this test (assuming that propagation ceases at 0.3 sec.) are shown in Figure 16. The corresponding

computed jet Karlovitz number (based on the smaller slot dimension) is given in Figure 17 at the time of flame impingement Its value is approximately 50.
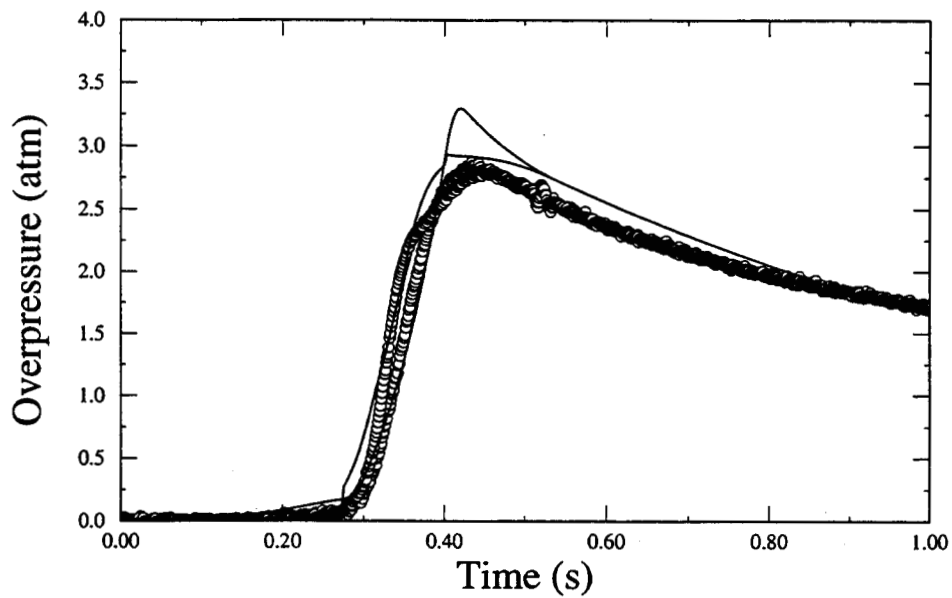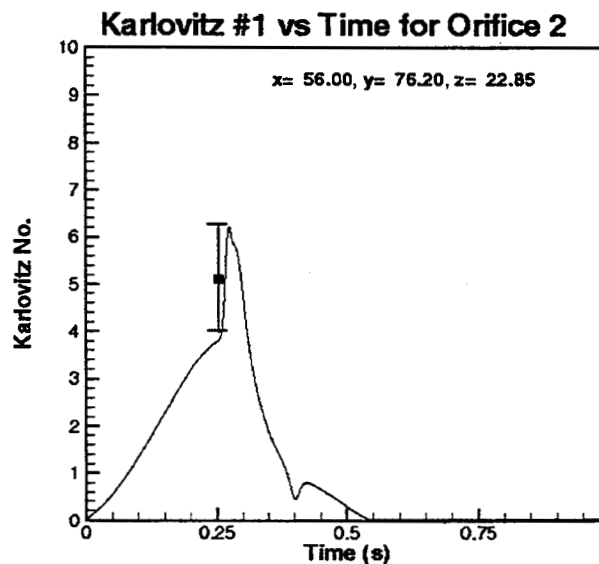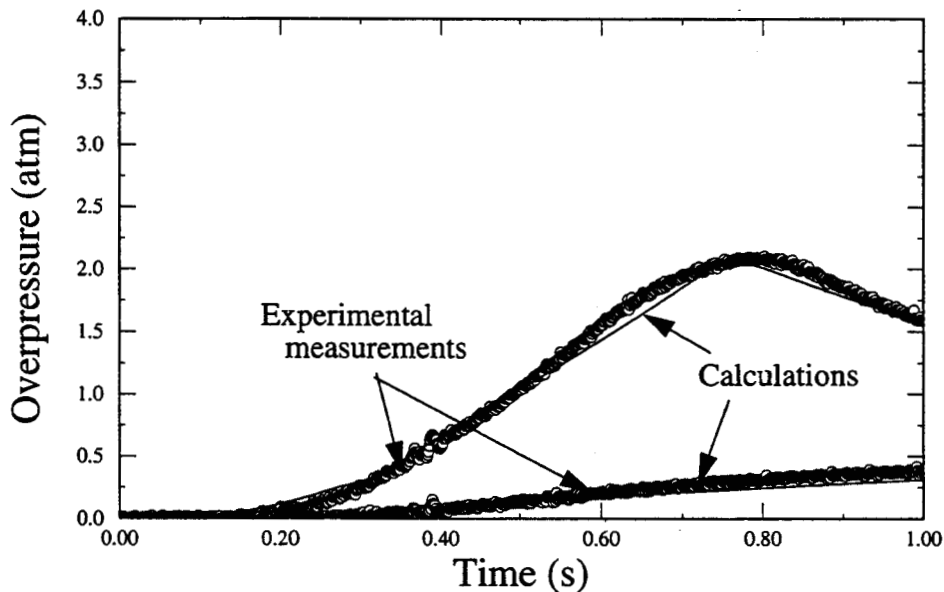

Figure 16. Overpressure versus time for Quarter-Scale Experiment 76
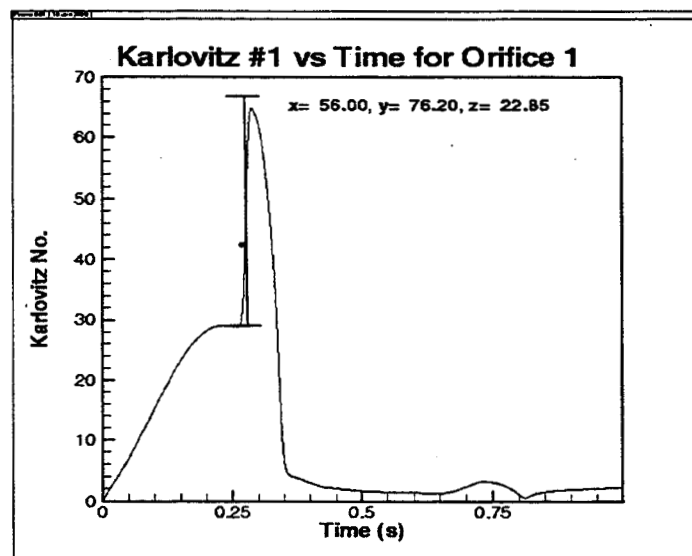
Figure 17. Jet Karlovitz number versus time for Quarter-Scale Experiment 76

Although a relatively small number of conditions were investigated in the two-compartment test series a possible quench criterion is suggested by determining a "critical" jet Karlovitz number at the time of flame impingement to the receiver chamber versus orifice diameter. The accumulative quench data is displayed in Figure 18. At 50 °C a jet Karlovitz number of approximately 3 separates

conditions where quench and sustained propagation is observed. A slightly higher value is suggested from tests conducted at 40 °C which is probably due to variations in the composition in the gaseous fuel-air mixture. (Perhaps additional scaling to the Zeldovich number is appropriate.) The error bars included on the data correspond to the range of Karlovitz number at the arrival time of flame impingement. This criteria is based on a very limited set of experiments with the location of the ignition point fixed for all conditions. Furthermore, these conditions apply to only a single orifice configuration. As one might expect, a different ignition location may yield different flow states and turbulence levels. Hence, there is much uncertainty associated with this quench criteria. Despite this questionable basis, an assessment of quench behavior in the full scale geometry can be done by monitoring the flow states at all of the orifice locations in the CWT configuration. The next section provides an assessment of possible quench behavior in a simulation of the full scale fuel tank.
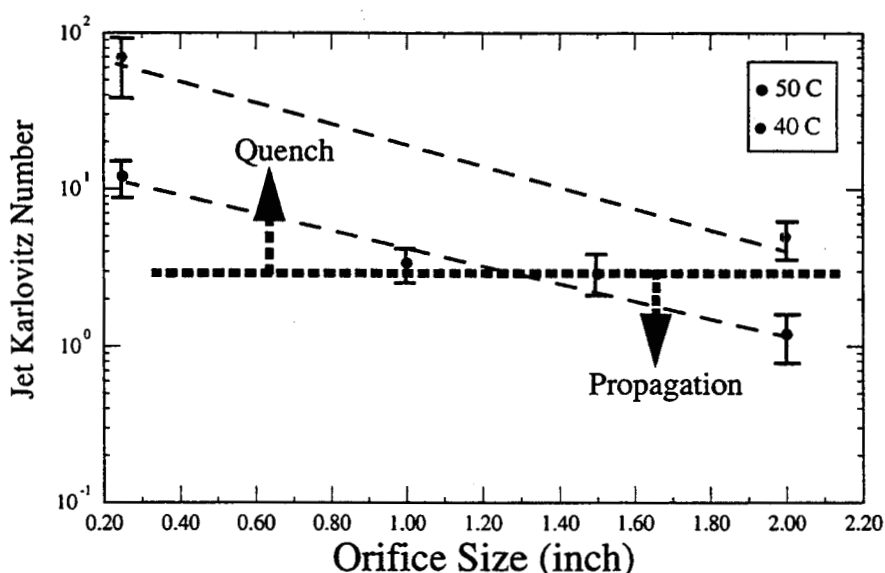

Figure 18. Jet Karlovitz number versus orifice size

Full-Scale Simulations

As a numerical experiment, a simulation of the combustion event in the full-scale Boeing 747 center wing fuel tank was conducted including all orifice connections between fuel compartments. In the quarter-scale model, many of the smaller orifices were consolidated, and the orifice flow area of the smaller orifices was combined with the nearest orifice neighbor. In some cases, the distance to the smallest orifice's nearest neighbor is large. If quench is not considered in the calculations, the orifices corresponding to actual locations trigger flame propagation at different times compared to a quarter-scale model, leading to significantly different results. Overpressures for a full-scale simulation are shown in Figure 19. The reference laminar burn velocity used was fixed at 37 cm/sec and the convection heat transfer coefficient was set at 30,000 erg/(cm^2 sec). (This value is purposely set low to provide an upper bound on the overpressure. A full-scale test is necessary to truly define a proper value for the convective heat loss.) Ignition is assumed to occur in compartment 2 at the vicinity of the fuel compensator. Near this ignition location there is a small orifice (which is absent in the quarter

scale model), connecting compartment 2 and compartment 4. As one might expect, this leads to accelerated burning in compartment 4 earlier than in a comparable quarter-scale configuration. As a result, flame propagation in compartment 4 triggers combustion in compartment 3 quickly due to the close proximity of a connecting orifice to the ignition location. Hence, the intercompartment pressures are similar if quenching does not occur. This simulation demonstrates that the location of intercompartment vents are important aspects in determining flame propagation paths within the tank configuration.

Another full-scale simulation is given in Figure 20 for a different ignition location in compartment 5. All input parameters remained the same as in the prior simulation and no quenching is considered in the calculation. The flame propagation in this simulation is different than ignition in compartment 2. The onset of rapid pressure rise for the case of ignition in compartment 5 is about 0.23 sec. as opposed to 0.20 sec. for the case of ignition in compartment 2. This difference is due to the relative isolation of the ignition point in compartment 5 to the nearest orifice location which can trigger accelerated burning. As a result, different compartment pressures develop which can lead to different structural loading on the internal walls of the CWT. The differential pressures are given in Figures 23 and 24. The pressure difference between compartments 3 and 4 for the two cases, shown in Figures 23d and 24d, illustrate some of the differences. The magnitude of the pressure differences for ignition in compartment 5 is greater than that for ignition in compartment 2.

Tables 1 and 2 provide the time of flame impingement and the corresponding flow characteristics of orifice velocity, pressure difference, and jet Karlovitz number at the various orifice locations in the full scale geometry. A negative pressure difference and orifice velocity implies that the flame is propagating into a compartment with a higher pressure. For such conditions, the flame front propagates toward an opposing jet flow before it reaches the orifice. As one expects, when the flame velocity is lower than the opposing jet flow the flame most likely extinguishes. Flame propagation toward an opposing flow did not occur in the two compartment tests so this blow off behavior was not experimentally investigated. Flame propagation at orifice locations having an impingement Karlovitz number greater than one or toward an opposing high speed flow may potentially be quenched, and in these full-scale simulations there are many such orifices. These simulations demonstrate that quench behavior is a probable event even in the full scale CWT.

Another full-scale simulation was performed in which the full-scale geometry incorporates the number of orifices and their placement corresponding to that of the quarter-scale tests. These results are depicted in Figure 21. As implied above, the timing of events, and the flame propagation path greatly differs from that of using the actual number of orifices and locations. Rapid pressure rise occurs after 0.30 sec., and in compartment 1 the peak pressure is not reached until 0.40 sec. The pressure differences for this case are shown in Figure 25, and they exhibit significantly different behavior compared to the two previous cases. For example, the pressure difference between compartment 5 and 6 experiences a negative phase whereas in the two previous cases they were always positive. The pressure difference is also greater. This difference may be representative of what would occur if the smaller holes in the full-scale fail to propagate flames, suggesting that quench behavior significantly alters the pressure history. In this simulation, as given in Table 3, fourteen of the orifices highlighted in this simulation have impingement jet Karlovitz numbers greater than one and are potential candidates for locations where quench behavior is possible.

A fourth full-scale simulation was performed which used the same geometry as the full-scale simulation with ignition in Compartment 2, but quenched combustion was considered. Two criteria were used to quench an impinging burn front. If the jet Karlovitz number at the time of impingement was greater than 1.5, then flame propagation was not allowed to transfer through the orifice. Also, if the pressure gradient across the orifice is negative, *i.e.* the pressure in the "from" compartment is less than the pressure in the "to" compartment, flame propagation is not triggered at the orifice since the orifice flow velocity usually greatly exceeds the burn velocity. Hence, the burn front never propagates through the orifice. The overpressures in the multiple tank compartments are given in Figure 22. Note that the time scale in Figure 22 is three seconds, as opposed to one second, underscoring the additional time for complete combustion within the domain to occur when quench occurs. In this simulation, eventually all the compartments burned because breakup of the flames is not modeled. *Only seven orifices propagated a flame while forty-two quenched.* Pressure differences between compartments are surprisingly similar in some cases, as displayed in Figures 23a and 26a. However, other compartments overpressures are distinctly different, such as those between compartments 5 and 6 (Figures 23c and 26c). In the absence of quench behavior, pressure difference are mostly positive and of the order 0.1 atm. With quench behavior, the pressure differences (see Figure 26c) have both large positive and negative phases with amplitudes of the order 1.0 atm. It is interesting to note that if the quench criteria had been lowered from 1.5 to 1.25, additional quench may have occurred and some compartments may not have had any flame propagation. This is consistent with observations in the quarter-scale Jet-A fuel experiments. Clearly, a more definitive basis for quench behavior is needed to assess the flame propagation behavior in the full scale fuel tank.

As a final simulation, an additional study was performed to address the issue of numerical grid resolution in the interface tracking algorithm. A coarse grid (16 cm on a side, with no grid refinement) was initially used to determine flame location. The numerical grid is then refined by a factor of eight and the results are compared to those of the previous simulation. A comparison of a typical pressure history at different numerical resolution is shown in Figure 27. This process was repeated until the overpressures for all six compartments changed by less than 0.5%. The characteristic spatial scale at which this convergence is achieved is 1 cm, which implies that an adequately resolved numerical solution requires a constant grid (as opposed to adaptively refined grid) consisting of over 50 million computational cells. This numerical requirement only applies to the interface tracking as opposed to resolving detailed fluid dynamic effects. It is likely that finer cell resolution is required to resolved detailed flow effects, particularly near small orifices.
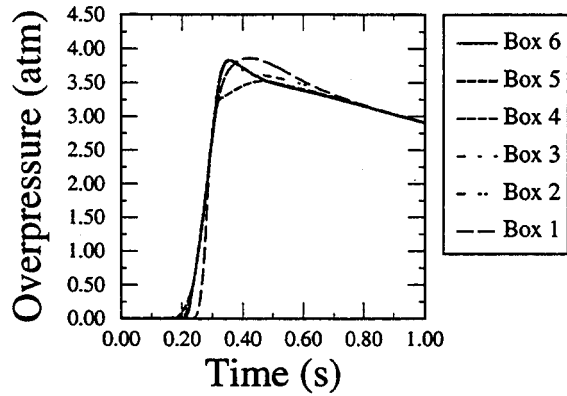
Figure 19. Overpressure versus time
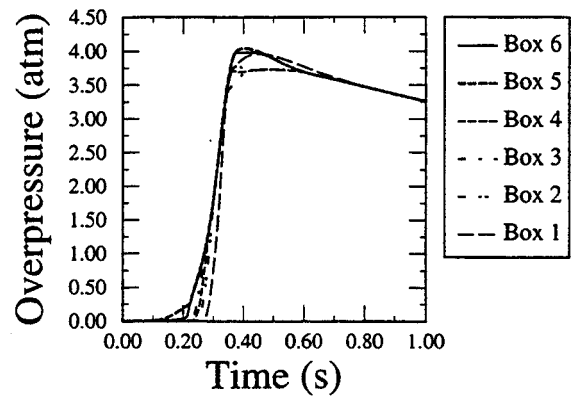for Full-Scale, Ignition in Bay 2

Figure 20. Overpressure versus time
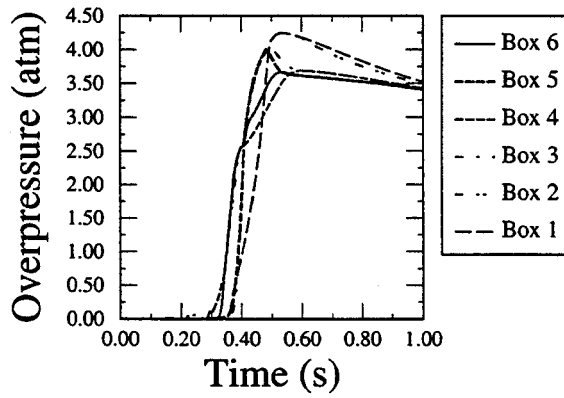for Full-Scale, Ignition in Bay 5

Figure 21. Overpressure versus time for Full-
Scale, Ignition in Bay 2, Orifice locations
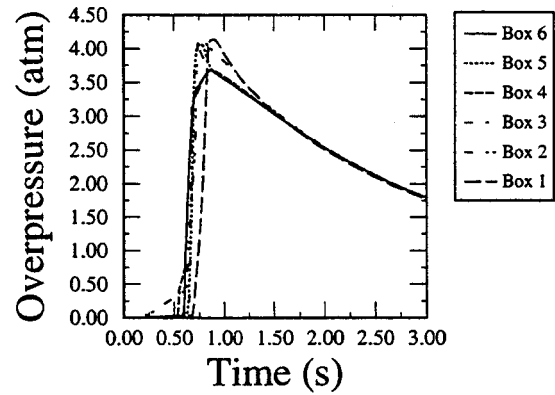based on quarter-scale configuration

Figure 22. Overpressure versus time for
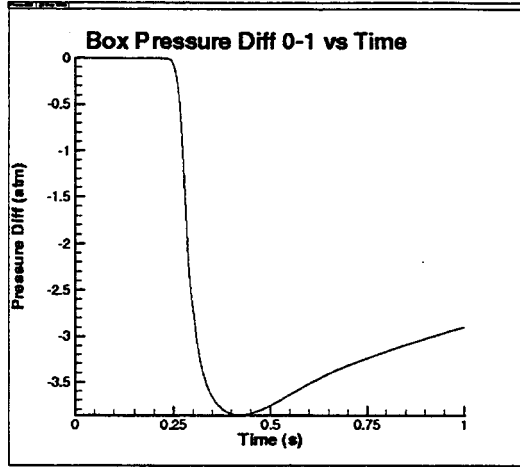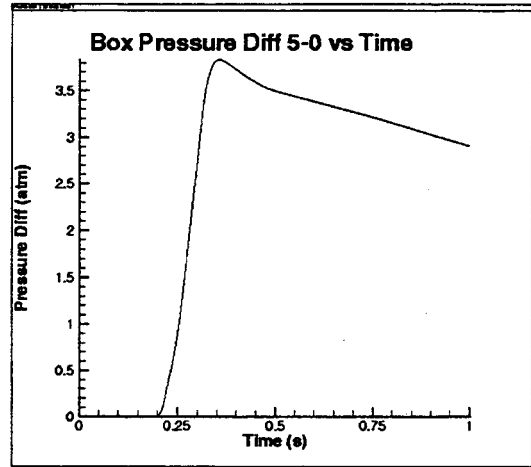Full-Scale, Ignition in Bay 2, Quench
based on Karlovitz number and blow-off
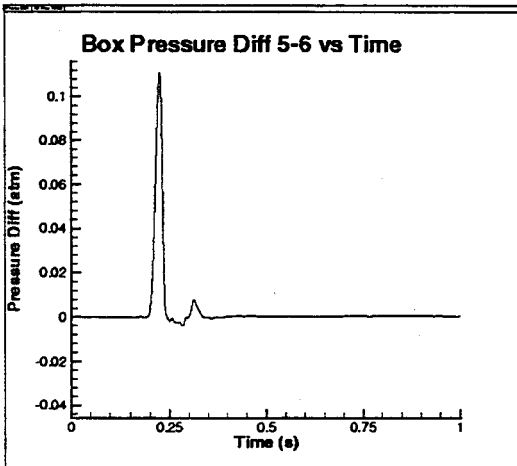
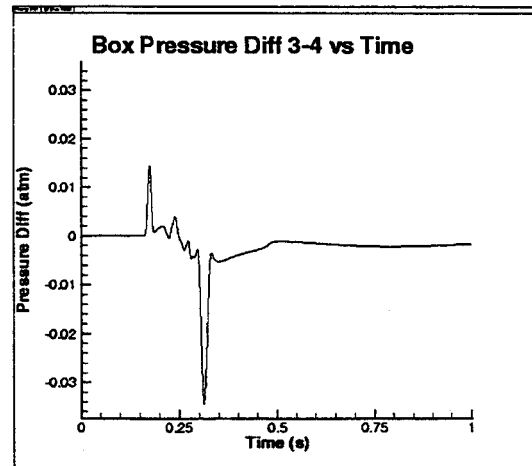Figure 23a

Figure 23b

Figure 23c

Figure 23d

Figure 23e

Figure 23f

Figure 23. Pressure Differences versus time for Full-Scale, Ignition in Bay 2

Page 28
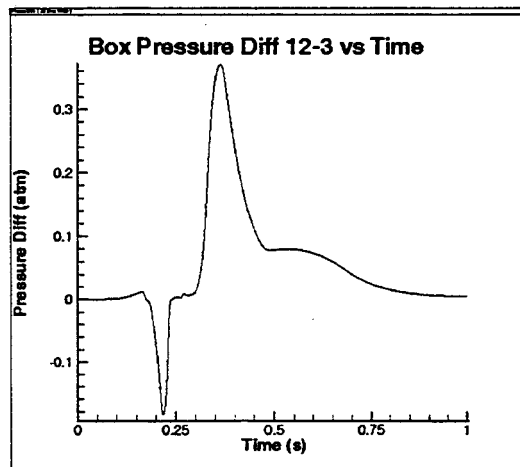
Figure 23g

Figure 23h
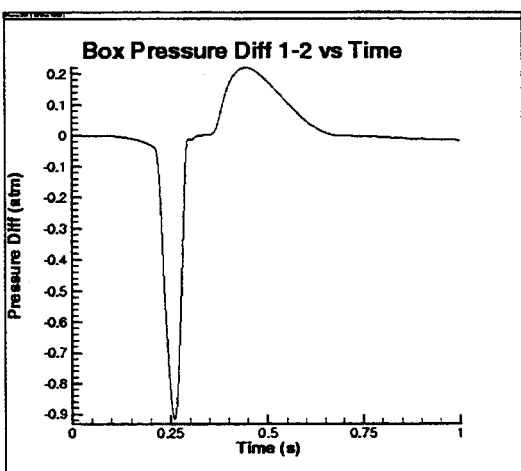
Figure 23i
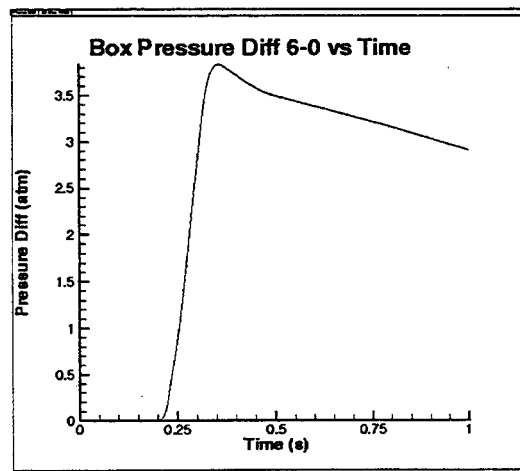
Figure 23j

Figure 23. Pressure Differences versus time for Full-Scale, Ignition in Bay 2
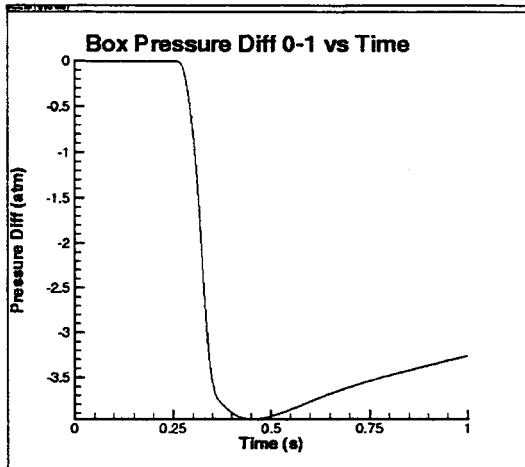
Figure 24a
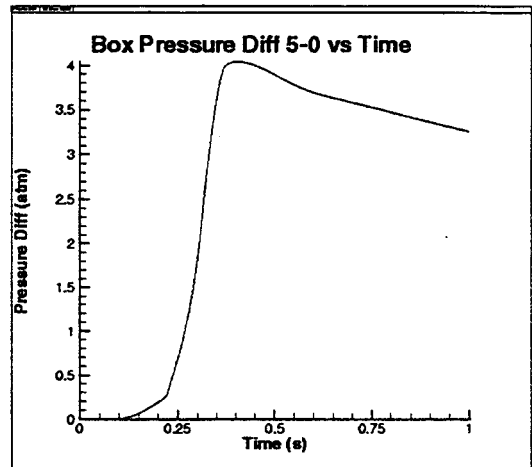
Figure 24b
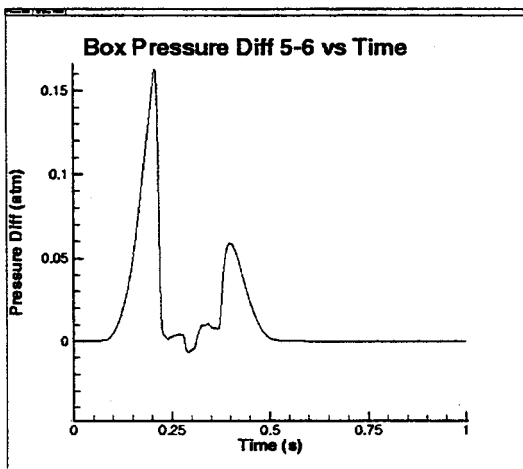
Figure 24c
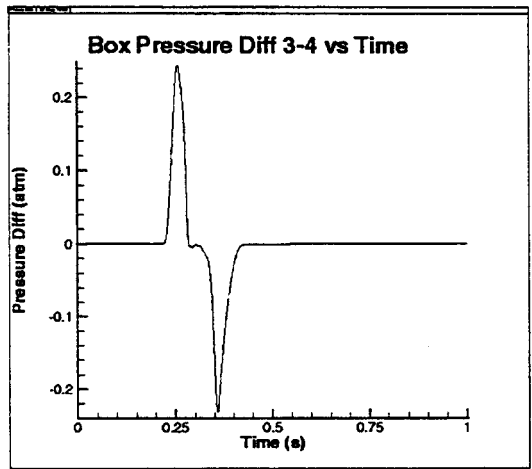
Figure 24d
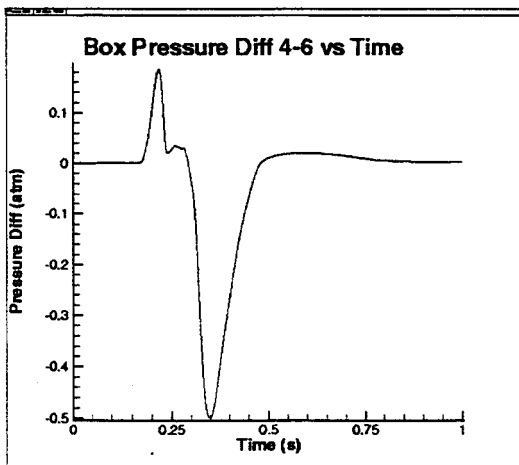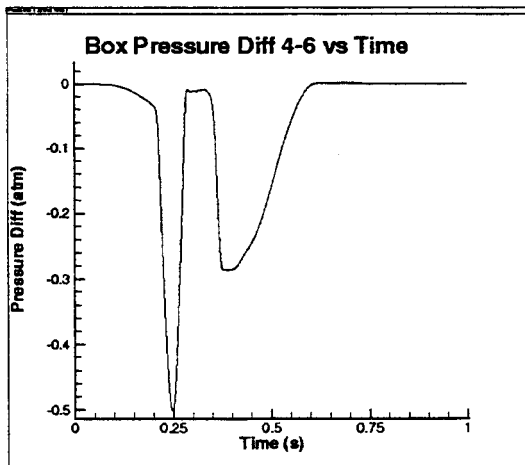

Figure 24e
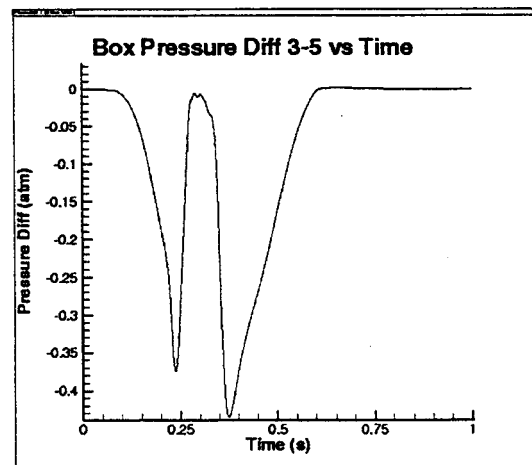
Figure 24f

Figure 24. Pressure Differences versus time for Full-Scale, Ignition in Bay 5
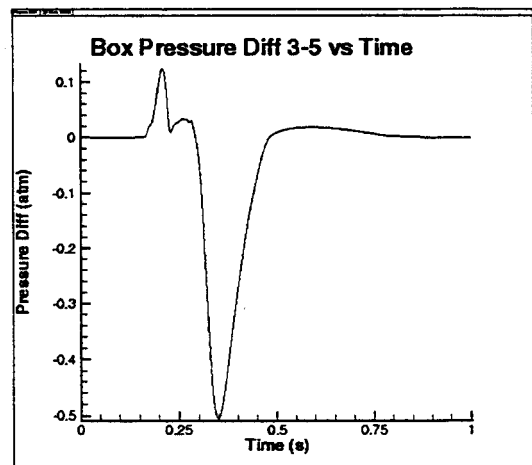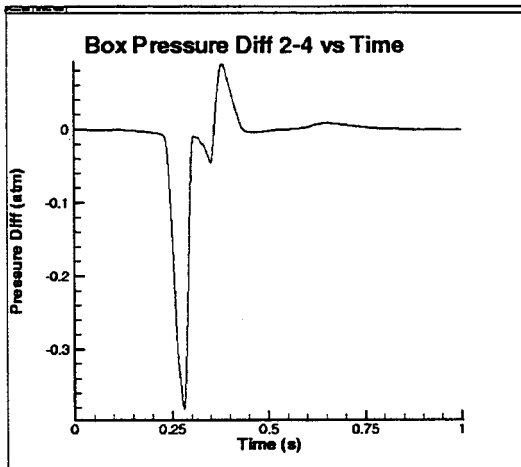
Figure 24g
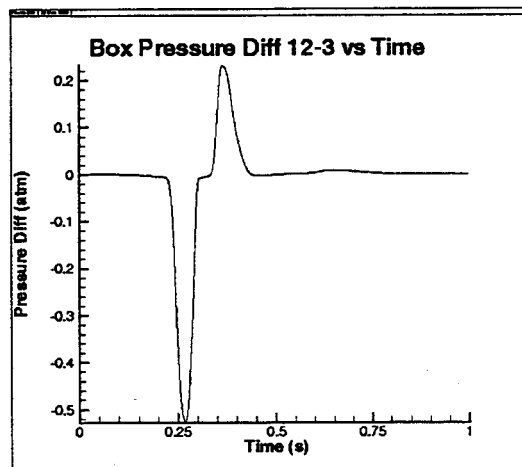
Figure 24h
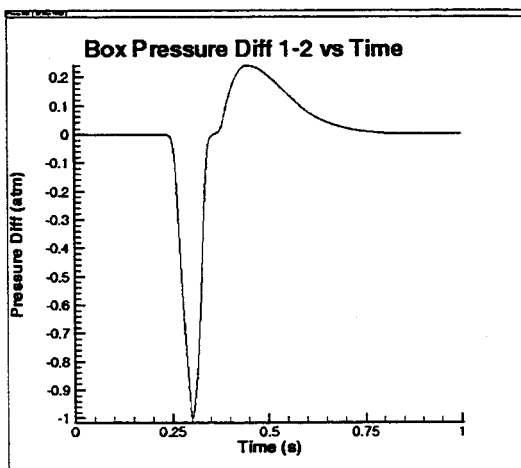
Figure 24i
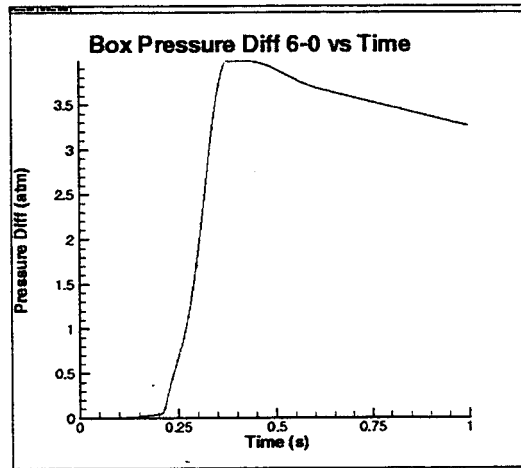
Figure 24j

Figure 24. Pressure Differences versus time for Full-Scale, Ignition in Bay 5
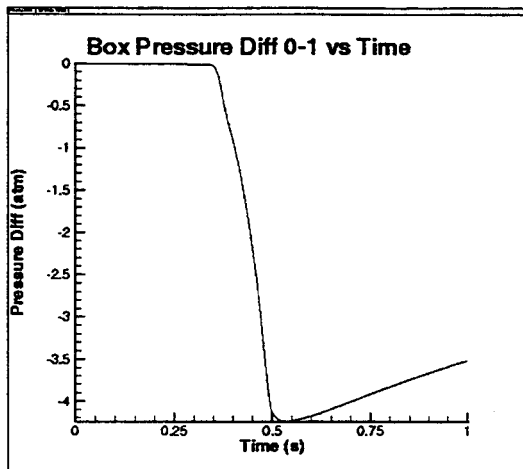
Figure 25a
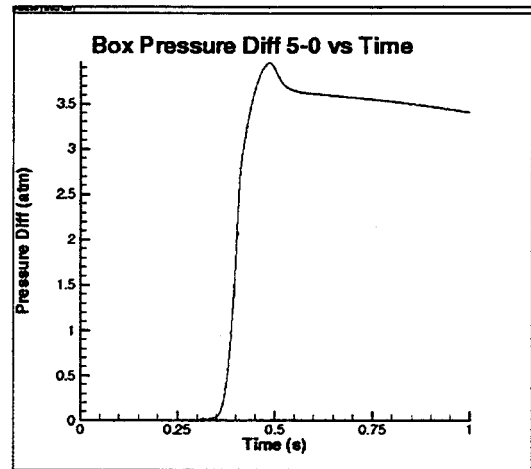
Figure 25b
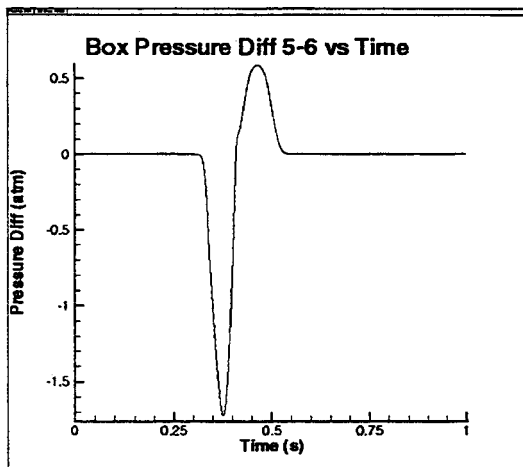
Figure 25c
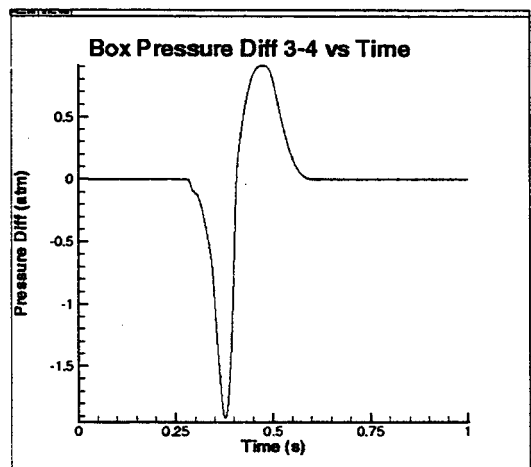
Figure 25d
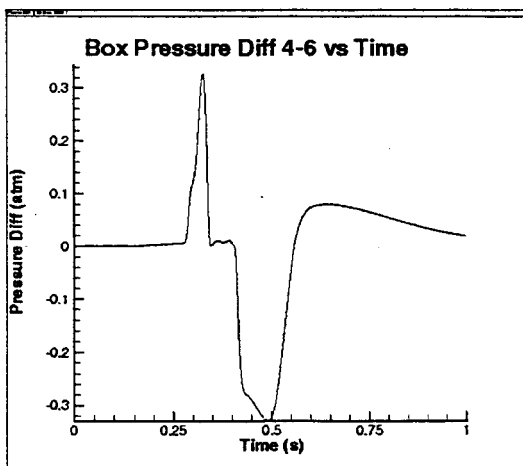
Figure 25e
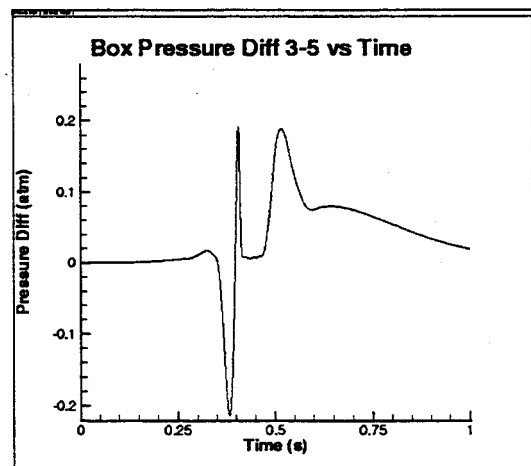
Figure 25f

Figure 25. Pressure Differences versus time for Full-Scale, Orifices from quarter-scale
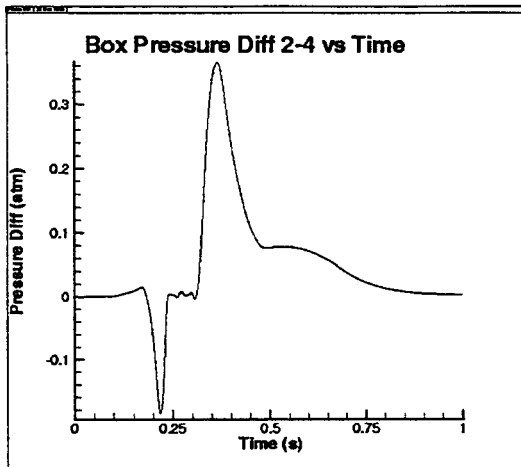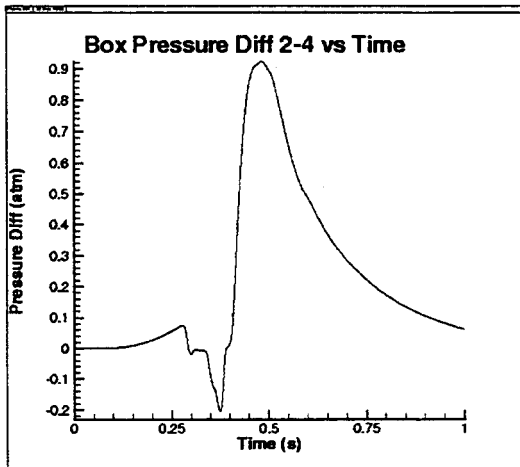
Figure 25g
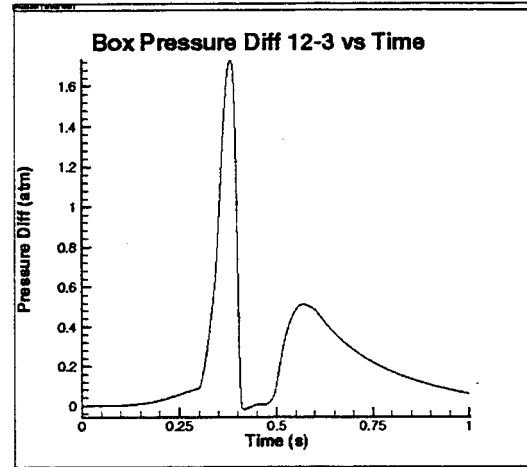
Figure 25h
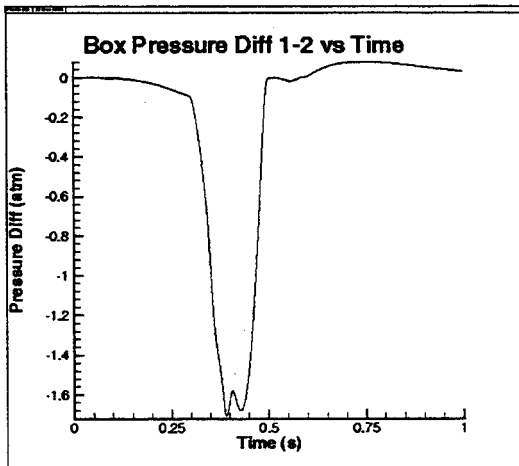
Figure 25i
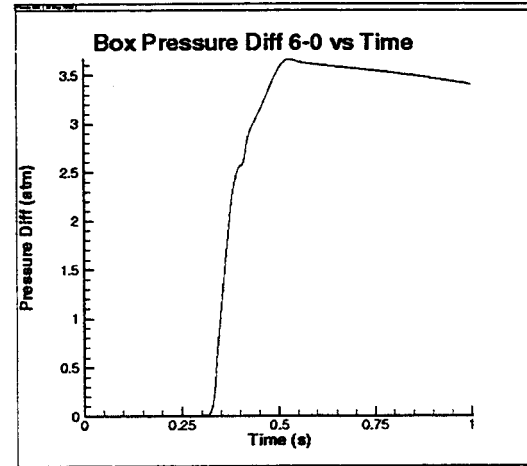
Figure 25j

Figure 25. Pressure Differences versus time for Full-Scale, Orifices from quarter-scale

Box Pressure Diff 0-1 vs Time

Figure 26a

Box Pressure Diff 5-0 vs Time

Figure 26b

Box Pressure Diff 5-6 vs Time

Figure 26c

Box Pressure Diff 3-4 vs Time

Figure 26d

Box Pressure Diff 4-6 vs Time
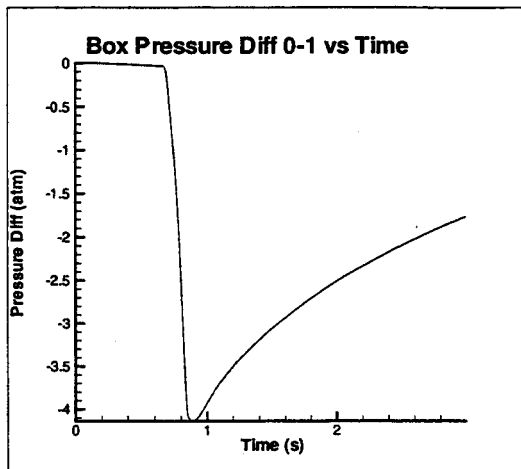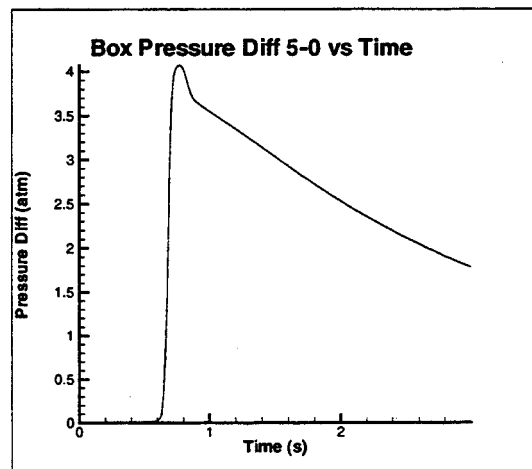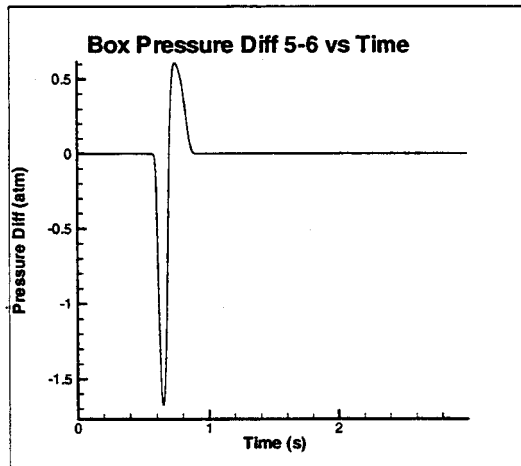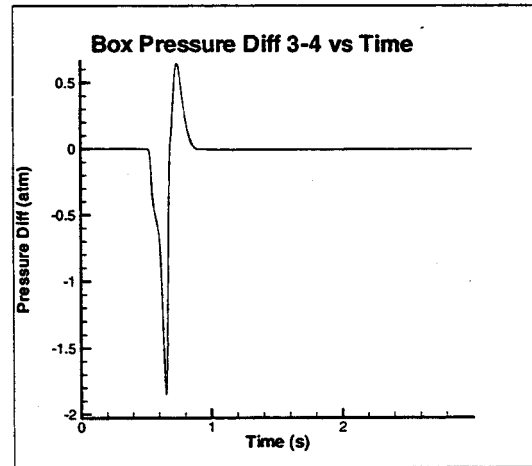
Figure 26e
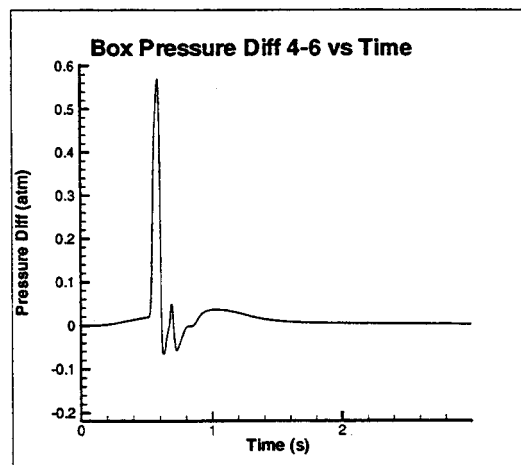
Box Pressure Diff 3-5 vs Time
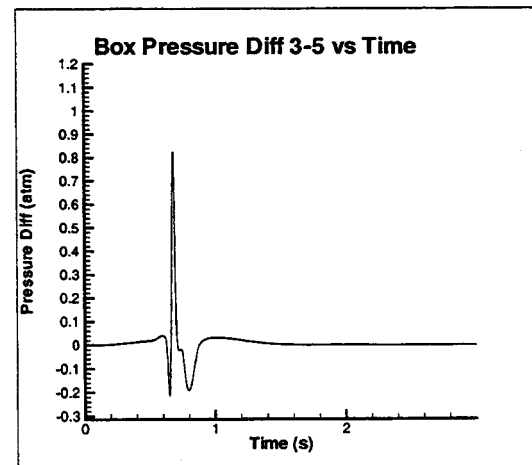
Figure 26f

Figure 26. Pressure Differences versus time for Full-Scale, Ignition in Bay 2
Quench based on Karlovitz number and blow-off

Box Pressure Diff 2-4 vs Time

Figure 26g

Box Pressure Diff 2-3 vs Time

Figure 26h

Box Pressure Diff 1-2 vs Time

Figure 26i

Box Pressure Diff 6-0 vs Time
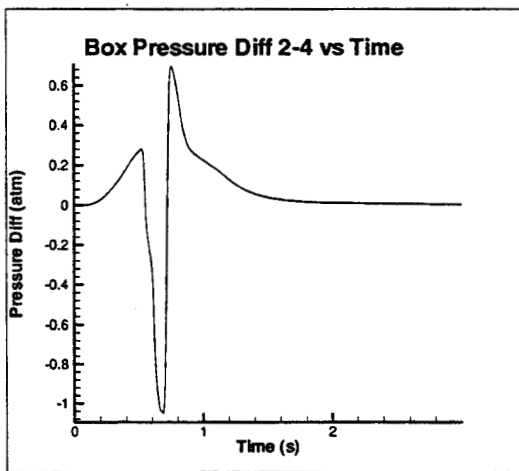
Figure 26j

Figure 26. Pressure Differences versus time for Full-Scale, Ignition in Bay 2
Quench based on Karlovitz number and blow-off

Compartment 1
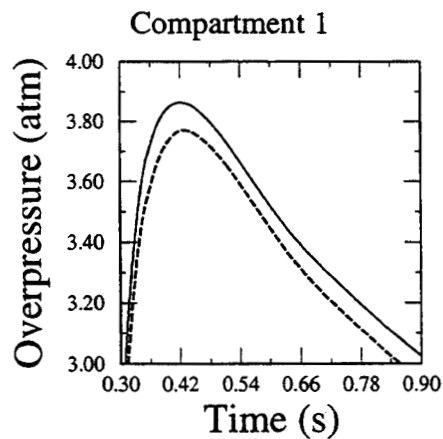
Figure 27. Overpressure versus time for Full-Scale, low versus high resolution

Table 1: Conditions at Flame Impingement - Ignition Bay 2[a]

Orifice no	Bay	Ignition Sequence	time sec.	$\mathcal{K}_{jet}$	Δp (atm.)	V(m/s)
1	6	55	0.302	0.04	-0.0415	-45.34
2	6	58	0.308	0.06	-0.0654	-51.02
5	6	23	0.226	0.72	0.1503	109.01
6	6	29	0.227	**1.83**	0.1505	106.25
9	4	42	0.261	0.55	-0.0454	-52.64
10	4	50	0.279	0.20	-0.0352	-43.80
13	5	5	0.197	3.5	0.0732	88.87
19	6	15	0.221	0.44	-0.0766	-82.41
20	3	17	0.222	**1.22**	-0.766	-82.41
21	3	59	0.315	0.06	0.0956	73.73
22	3	60	0.330	0.10	0.3875	99.50
26	4	39	0.235	0.06	0.0060	12.68
28	2	45	0.269	0.06	-0.0244	-35.24
29	2	61	0.330	0.06	-0.1513	-64.78
30	2	54	0.301	0.07	-0.0045	-21.10
32	2	20	0.223	**1.44**	0.1796	113.72
33	3	1	0.165	**3.25**	0.0129	41.55
35	3	37	0.232	0.40	-0.0912	-86.70
36	3	51	0.280	0.04	-0.0171	-8.59
40	2	12	0.216	**1.77**	0.1804	115.41
43	2	43	0.267	0.06	-0.0154	-35.12
44	2	56	0.304	0.01	-0.0039	-4.74
45	2	57	0.306	0.02	0.0083	14.89
47	2	53	0.297	0.03	0.0141	8.82
49	2	41	0.255	0.59	-0.8780	-143.04
51	2	44	0.267	0.89	-0.8949	-148.13
52	2	49	0.271	0.39	-0.8264	-148.84
53	2	52	0.287	0.15	-0.2297	-93.74
55	1	62	0.334	0.01	0.0048	11.34
57	1	40	0.249	**3.41**	0.7771	140.37

Table 1: Conditions at Flame Impingement - Ignition Bay 2[a]

Orifice no	Bay	Ignition Sequence	time sec.	$\mathcal{K}_{jet}$	Δp (atm.)	V(m/s)
59	1	38	0.233	**3.62**	0.3799	131.41
63	6	6	0.204	0.36	0.0084	30.95
64	6	7	0.204	0.39	0.0099	33.97
66	6	9	0.209	0.67	0.0299	58.98
68	6	11	0.27	0.85	0.0596	79.10
71	6	15	0.221	**2.1**	0.1031	95.64
72	6	18	0.223	**1.96**	0.1116	97.43
73	6	19	0.223	**1.76**	0.1116	97.43
75	6	27	0.227	0.83	0.1152	96.78
77	6	28	0.227	0.83	0.1152	96.78
79	6	33	0.227	0.81	0.1137	96.17
85	5	8	0.207	0.54	-0.0207	-49.63
87	5	10	0.212	0.69	-0.0429	-69.35
89	5	13	0.218	0.74	-0.0826	-89.40
90	5	14	0.221	0.33	-0.1031	-95.64
94	5	35	0.230	0.47	-0.1025	-90.62
96	5	26	0.227	0.67	-0.1152	-96.78
98	5	34	0.229	0.60	-0.1068	-93.00
100	5	32	0.227	0.55	-0.1137	-96.17
101	5	30	0.227	0.55	-0.1137	-96.17
102	5	31	0.227	0.82	-0.1137	-96.17
105	4	2	0.174	0.48	0.0136	40.31
107	4	25	0.226	0.15	0.0144	22.94
109	4	22	0.225	0.11	0.0056	22.56
111	3	4	0.184	0.27	-0.0026	-24.27
112	3	3	0.179	0.37	-0.0146	-45.07
114	3	36	0.232	0.10	-0.0163	-23.92
116	3	24	0.226	0.15	-0.0144	-22.94
118	3	21	0.225	0.11	-0.0056	-22.56

a. Bold Face denotes Karlovitz number greater than one and possible quench

Table 2: Conditions at Flame Impingement - Ignition Bay 5[a]

Orifice no	Bay	Ignition Sequence	time sec.	$\mathcal{K}_{jet}$	Δp (atm.)	V(m/s)
3	6	41	0.284	0.16	0.0124	16.14
4	6	44	0.305	0.11	0.0271	25.13
7	4	46	0.314	0.02	-0.0294	-20.33
8	4	50	0.322	0.06	0.0199	42.02
11	4	30	0.255	0.80	0.4797	138.08
12	4	28	0.253	**2.43**	0.5006	138.31
15	5	26	0.246	**1.22**	-0.3441	-130.92
16	5	57	0.344	0.03	-0.1105	-49.15
17	5	59	0.351	0.07	-0.1984	-73.64
18	3	21	0.222	**4.87**	0.2485	125.29
19	3	27	0.247	0.72	0.3333	130.60
25	4	52	0.328	0.04	-0.0041	-14.09
26	4	42	0.285	0.24	-0.3642	-124.88
28	2	49	0.320	0.03	0.0294	29.37
29	2	58	0.348	0.03	0.0349	33.87
32	2	37	0.264	**1.33**	0.2991	127.30
35	3	39	0.276	0.31	-0.5032	-138.41
36	3	43	0.301	0.19	-0.0322	-40.72
39	2	25	0.241	**8.52**	0.1468	110.74
40	2	29	0.255	**2.02**	0.4314	134.48
43	2	45	0.312	0.03	-0.0007	-25.09
44	2	47	0.317	0.03	-0.0110	-17.88
45	2	55	0.341	0.07	-0.0931	-55.92
47	2	53	0.336	0.22	-0.2162	-82.79
51	2	48	0.317	0.51	-0.8271	-146.37
52	2	51	0.323	0.20	-0.6644	-135.32
55	1	60	0.357	0.01	0.0044	11.89

Table 2: Conditions at Flame Impingement - Ignition Bay 5[a]

Orifice no	Bay	Ignition Sequence	time sec.	$\mathcal{K}_{jet}$	Δp (atm.)	V(m/s)
57	1	40	0.284	**2.50**	0.6945	141.08
58	1	31	0.259	**1.85**	0.1118	100.17
59	1	38	0.272	**3.39**	0.4303	133.42
62	1	54	0.339	0.07	0.1281	64.08
63	6	20	0.222	0.44	0.0306	62.61
65	6	12	0.217	0.86	0.1124	100.81
66	6	13	0.217	0.86	0.1124	100.81
68	6	14	0.217	0.86	0.1124	100.81
70	6	1	0.206	0.56	0.1619	113.12
72	6	3	0.212	**2.71**	0.1617	113.18
75	6	5	0.213	**1.30**	0.1549	111.70
76	6	6	0.213	**1.30**	0.1549	111.70
78	6	8	0.216	**1.11**	0.1266	104.84
79	6	9	0.216	**1.11**	0.1266	104.84
81	6	16	0.219	0.74	0.0872	92.10
82	6	17	0.219	**1.11**	0.0872	92.10
84	5	19	0.222	0.41	-0.0306	-62.61
87	5	11	0.217	0.67	-0.1124	-100.81
89	5	18	0.221	0.49	-0.0504	-74.98
91	5	2	0.212	**1.88**	-0.1617	-113.18
93	5	4	0.213	**1.65**	-0.1549	-111.70
94	5	10	0.217	0.69	-0.1198	-103.00
97	5	7	0.216	0.84	-0.1266	-104.84

a. Bold Face denotes Karlovitz number greater than one and possible quench

Table 3: Conditions at Flame Impingement - Scaled-up Orifices[a]

Orifice no	Bay	Ignition Sequence	time sec.	$\mathcal{K}_{jet}$	Δp (atm.)	V(m/s)
1	6	3	0.316	**1.22**	0.2252	123.21
2	6	3	0.316	**2.13**	0.2229	122.96
4	6	46	0.369	0.08	0.0601	37.23
8	4	19	0.364	0.05	0.0102	34.05
10	4	20	0.369	0.07	-0.0601	-37.23
12	5	26	0.373	**1.57**	-0.1571	-107.72
14	5	37	0.407	0.14	0.2684	91.39
15	3	25	0.373	0.82	0.1571	107.72
17	3	38	0.408	0.08	-0.2793	-93.39
19	4	1	0.280	**1.52**	0.0757	89.45
21	4	10	0.346	0.52	-0.0295	-52.13
23	4	4	0.316	0.32	-0.0043	-35.03
25	2	2	0.304	0.45	0.0265	53.87
27	2	6	0.317	0.10	-0.0074	-15.97
32	3	41	0.419	0.02	-0.0005	-21.49
33	3	39	0.416	0.02	0.0016	20.41
34	2	31	0.384	0.28	-1.7220	-155.91
35	2	36	0.397	0.15	-1.1336	-156.69
36	2	42	0.460	0.02	-0.0145	-10.79
43	2	40	0.417	0.35	-1.6253	-161.20
44	2	43	0.473	0.28	-0.8364	-136.22
46	2	44	0.491	0.05	-0.1585	-67.17
47	1	9	0.343	**3.69**	0.6546	137.42
48	1	15	0.357	**4.45**	1.1214	145.37
49	1	8	0.342	**2.30**	0.6395	137.31
50	1	7	0.342	**2.03**	0.6336	137.27
53	1	45	0.492	0.06	0.1422	63.96
55	6	14	0.357	0.10	-1.2451	-147.05

Table 3: Conditions at Flame Impingement - Scaled-up Orifices[a]

Orifice no	Bay	Ignition Sequence	time sec.	$\mathcal{K}_{jet}$	Δp (atm.)	V(m/s)
57	6	12	0.353	0.34	-1.0753	-145.02
60	6	21	0.369	0.11	-1.5915	-152.79
62	6	27	0.376	0.19	-1.7605	-155.93
65	6	29	0.381	0.18	-1.6866	-157.05
67	5	13	0.353	**1.51**	1.0798	145.10
69	5	11	0.349	**1.51**	0.9058	141.95
70	5	23	0.369	**1.31**	1.6187	152.84
72	5	24	0.369	**1.10**	1.6187	152.84
74	5	28	0.377	0.80	1.7447	156.21
75	5	30	0.381	0.63	1.6876	157.06
78	4	8	0.361	0.22	-1.4207	-149.36
80	4	35	0.396	0.17	-1.2164	-158.36
83	4	32	0.393	0.17	-1.4194	-158.99
84	3	18	0.361	**1.26**	1.4268	149.45
86	3	16	0.359	**1.26**	1.3772	148.40
88	3	33	0.394	0.39	1.3773	159.07
89	3	34	0.394	0.39	1.3773	159.07

a. Bold Face denotes Karlovitz number greater than one and possible quench

Summary and Conclusions

In this second phase of quarter-scale testing using heated jet fuel, both experimental measurements and modeling simulations have revealed that the combustion behavior of Jet-A fuel-air mixtures is different than the simulant fuel. Tests showed that explosions can result in such mixtures, however, the most distinguishing feature of the explosive event is the occurrence of quenched combustion. This quenching leads to different pressure loading within the fuel tank. There is still much to be learned about the mechanism and scaling rules of this combustion behavior.

A preliminary study of quenching was attempted by simplifying the tank configuration to two compartments to avoid addressing the complex flame propagation paths. Pressure measurements, by themselves, are not sufficient to resolve this behavior. Modeling provided a means for evaluating flow states associated with intercompartment propagation. Unfortunately, the simplification of geometry did not treat all possible flow states. A small number of experiments were conducted which produced a preliminary criteria for quench behavior. This study was not sufficient to establish a fundamental understanding of the mechanism of quench behavior. In light of the small number of experiments, modeling of the full scale has to be regarded with a great deal of uncertainty. At its current state, modeling can not provide a definitive tool in determining the location of the ignition in the CWT. The combustion behavior of actual jet fuel mixtures is far more complex than originally envisioned. The lack of definitive initial conditions and the weak basis of the current understanding of combustion behavior in multicomponent fuel-air mixtures lead to much uncertainty in the modeling.

References:

1. National Transportation Safety Board Investigative Hearing on TWA Flight 800, Baltimore, MD, December 8-12, 1997.

2. Berg, J. T., Ryum, S. R, and van Wingerden, K, "A Brief Description of the FLACS Ventilation, Dispersion and Explosion Simulator," Christian Michelsen Research Laboratory, Bergen, 1997.

3. Baer, M, R. and Gross, R. J, "A Combustion Model for the TWA 800 Center-Wing Fuel Tank Explosion," Sandia National Laboratories, SAND98-2043, 1998.

4. Abdel-Gayed, R. G., Bradley, D., et al., "Turbulent Burning Velocities: A General Correlation in Terms of Staining Rates," Proc. Roy. Soc. London, A 414, pp. 389-413, 1987.

5. Shepherd, J.E.,et al., "Jet A Explosions -Field Test Plan for 1/4 Scale Experiments,", California Institute of Technology Report FM97-17, Pasadena, CA, 1997.

6. Shepherd, J.E., et al., "Jet A Explosion Experiments: Laboratory Testing," California Institute of Technology Report FM97-9, Pasadena, CA, 1997.

7. Shepherd, J. E., et al., "Results of 1/4-Scale Experiments, Vapor Simulant and Liquid Jet A Tests," California Institute of Technology Report, FM98-6, 1998.

8. Bower, D.R., "Light Test Group Chairman's Factual Report of Investigation, NTSB Exhibit 23-A, Docket Number SA-516, NTSB Accident Investigation Number DCA96MA070, 1997.

9. Sagebield, J. C. "Sampling and Analysis of Vapors from the Center Wing Tank of a Test Boeing 747-100 Aircraft, Desert Research Institute, NTSB final report. 1997.

10. Dahn, J. C. et al., "Methodology to Evaluate Industrial Vapor and Dust Explosion Hazards, "International Symposium on Hazards, Prevention and Mitigation of Industrial Explosion proceedings, 1998.

11. Lewis, B. and von Elbe, G., **Combustion, Flames, Explosions of Gases**, Academic Press, NY, 1961.

12. Williams, F. A., **Combustion Theory, The Fundamental Theory of Chemically Reacting Flow Systems**, Benjamin/Cummings Pub. Company, Menlo Park, CA, 1985.

13. Bradley, D. "How Fast Can We Burn?," 24th Symposium (International) on Combustion, 1992, pp. 247-262.

14. Larsen, O, "A Study of Critical Dimensions of Holes for Transmission of Gas Explosions and Development and Testing of a Schlieren System for Studying Jets of Hot Combustion Products,", MSc Thesis, University of Bergen, Norway, 1998.

15. van Wingerden, K., Renoult, J., and Armond S., "CFD Gas Explosion Simulations to Support the Investigation into the Cause of the Explosion in the Center Wing Tank of TWA 800", Christian Michelsen Research Laboratory Report CMR-00-30026, April, 2000.

16. Hinze, J. O., **Turbulence**, 2nd Ed., McGraw-Hill Pub., New York, NY, 1975.

Distribution

External Distribution:

Applied Research Associates   (4)
5941 S. Middlefield Road, Suite 100
Littleton, CO 80123
Attn: Mr. Peter T. Dzwilewski
     Mr. Larry L. Brown
     Mr. Robert L. Guice
     Mr. Tim Samaras

Dr. Merritt M. Birky
Office of Research and Engineering
National Transportation Safety Board
490 L'Enfant Plaza, S.W.
Washington, D.C. 20594

Dr. Daniel R. Bower
Office of Research and Engineering
National Transportation Safety Board
490 L'Enfant Plaza , S.W.
Washington, D.C. 20594

Mr. Dennis A. Crider
Office of Research and Engineering
National Transportation Safety Board
490 L'Enfant Plaza , S.W.
Washington, D.C. 20594

Dr. Vern Ellingstad
Office of Research and Engineering
National Transportation Safety Board
490 L'Enfant Plaza , S.W.
Washington, D.C. 20594

Dr. Jim Hall
National Transportation Safety Board
490 L'Enfant Plaza , S.W.
Washington, D.C. 20594

Dr. J. Christopher Krok
California Institute of Technology
Mail Stop 205-45
Pasadena, CA 91125

Dr. Julian J. Lee
California Institute of Technology
Mail Stop 301-46
Pasadena, CA 91125

Prof. Joseph E. Shepherd
California Institute of Technology
Mail Stop 105-50
Pasadena, CA 91125

Dr. Paul Thibault
Combustion Dynamics Ltd.
Suite 301, 1888 Brunswick St.
Halifax, Nova Scotia
B3J 3J8

Dr. Kees van Wingerden
Christian Michelson Research AS
Fantoftvegen 38, P.O. Box 3
N-5036 Fantoft, Bergen, Norway

Leo D. Budd
Commander
NAWCWPNS
1 Administration Circle
China Lake, CA 93555-6100

Martin L. Lentz
AFRL/VAVS (WL/FIVS) Bldg 63
1901 Tenth Street
WPAFB, OH 45433-7605

Michael J. Clauson
US Army Tank Automotive and
     Armaments Command
Attn: AMSTA-TR-R / 263 (Mr. Clauson)
Warren, MI 48397-5000

Thor Eklund
119 North Drive
Haddonfield, NJ 08033

Thomas L. Wasmund
Code G24
Naval Surface Warfare Center
Dahlgren Division
17320 Dahlgren Road
Dahlgren, VA 22448-5100

Hugh Griffis
NASC/XRA, Bldg 16
2275D Street, Suite10, Room 0067
Wright Patterson AFS, OH 45433-7227

Internal Distribution:

Copy to:

MS 0449	5300	Ellis, D.E.	
MS 0841	9100	Bickel, T.C.	
MS 0836	9100	Baer, M.R.	(10)
MS 0824	9110	Ratzel, A.C.	
MS 0826	9113	Hermina, W.	
MS 0834	9114	Johannes, J.	
MS 0825	9115	Rutledge, W.H.	
MS 0836	9116	Hertel, E.	
MS 0836	9116	Gross, R.J.	(20)
MS 0827	9117	Griffith, R.O.	
MS 0835	9120	Morgan, H.S.	
MS 0824	9130	Moya, J.L.	
MS 0828	9132	Tieszen, S.R.	
MS 0835	9142	Peery, J.S.	
MS 9018	8940-2	Central Tech Files	
MS 0899	4916	Technical Library	(2)
MS 0612	4912	Review & Approval Desk For DOE/OSTI	